DESIGN, FABRICATION, AND TESTING OF A SHAPE MEMORY POLYMER BASED PATENT DUCTUS ARTERIOSUS CLOSURE DEVICE

A Dissertation

by

MARK ALLEN WIERZBICKI

Submitted to the Office of Graduate and Professional Studies of
Texas A&M University
in partial fulfillment of the requirements for the degree of

DOCTOR OF PHILOSOPHY

Chair of Committee,	Duncan J. Maitland
Committee Members,	John C. Criscione
	Balakrishna Haridas
	Matthew W. Miller
Head of Department,	Anthony Guiseppi-Elie

May 2017

Major Subject: Biomedical Engineering

ABSTRACT

Patent ductus arteriosus (PDA) is a congenital cardiovascular defect in which a fetal connection between the aorta and pulmonary artery does not close spontaneously shortly after birth. This defect is the most common congenital cardiovascular abnormality found in canines and when left uncorrected can result in serious complications and even death. In the dog, PDA has been historically corrected via surgical ligation, however minimally invasive options, namely the Amplatz® Canine Ductal Occluder (ACDO), have become the preferential closure method when available. However, while effective, use of the ACDO can be limited by its relatively large delivery system size and cost. Thus, an alternative device that addresses these limitations is desired.

Shape memory polymer (SMP) foams are a unique class of materials that have promising applications in the field of minimally invasive occlusion devices. A prototype nitinol foam cage (NFC) device designed using these materials and nitinol has been constructed to treat and occlude canine PDA. The first iteration of the NFC was evaluated using mechanical and *in vitro* experiments to assess its performance compared to that of a commercial ACDO. While the results were promising, with the prototypes showing lower radial pressure than the ACDO, and exhibiting limited migration *in vitro,* improving the stability and fit within the PDA geometry was desired. Design alterations to the nitinol frame and amount of foam used were implemented to address these concerns. Verification tests of this prototype, included fatigue, radial force, stability, and ease of deployment assessments. The prototypes exhibited promising initial fatigue characteristics, generated

lower wall tensions, and exhibited similar stability and delivery characteristics compared to the ACDO. The results showed promising potential that with minimal refinement, the prototype NFC could be used for canine PDA closure.

A hydrogel clot mimic was designed for use with shape memory polymer foams to assess the performance of prototypes following foam occlusion without the complications of using blood. A polyacrylamide composition was selected in which the storage modulus of the hydrogel-clotted foam matched that of a blood-clotted foam. The utility of these materials was demonstrated in a verification test using the NFC which measured the force required to dislodge the prototype from the PDA with bare and hydrogel clotted foams.

DEDICATION

This dissertation is dedicated to my mother and father who have constantly provided me with love, support, and guidance throughout grad school and my entire life. Thank you, I love you both.

ACKNOWLEDGEMENTS

I would like to thank my committee chair, Dr. Duncan Maitland for supporting and guiding me through grad school. Dr. Maitland provided a well-equipped and collaborative lab environment to conduct research. The access to rapid prototyping equipment was invaluable for iterating on device designs, and improved the end-product that I was able to deliver. I thank him for recognizing my potential and advising me to pursue a PhD after starting in his lab as a Master's student. The opportunity to continue development of the PDA device to the point at which we could deliver these into animals has been a difficult, but exciting pursuit. I really appreciated his method of offering guidance and non-restrictive leadership. This allowed me to explore more ideas and feel a greater sense of ownership and pride of the work that I completed. I feel that his guidance has made me a better engineer and inventor.

I would like to thank my committee members, Dr. John C. Criscione, Dr. Balakrishna Haridas, and Dr. Matthew W. Miller for their help and guidance. Dr. Criscione provided assistance and advice regarding the radial force analysis of the devices, and his knowledge of mechanics greatly strengthened that experiment and segment of my dissertation. Dr. Matthew W. Miller originally pitched this project to Dr. Maitland, and provided initial input, recommendations, and testing on prototype design. Thank you for providing me with an ACDO and catheters I could use to evaluate and test my prototypes against. I greatly appreciate your expertise and help. Dr. Haridas increased my knowledge of medical device design and development.

Thank you to Dr. Sonya Gordon, Dr. Ashley Saunders, Scott Birch and the Texas A&M Veterinary Cardiology team. Their constructive input regarding the prototype and knowledge of PDA procedures was valuable to further development of the design. I have always enjoyed working with this group on this project and in other endeavors.

Thank you to all my friends and colleagues for their help designing and assisting with experiments and helping get through tough parts of grad school. The collaborative nature of everyone in the Biomedical Device Laboratory was instrumental in my development as an engineer. Thank you, Dr. Tony Boyle, Dr. Landon Nash, Dr. Todd Landsman, Dr. Andrew Weems, John Horn, Dr. Marziya Hasan, Dr. Wonjun Hwang, Jason Szafron, Jesse Bryant, Rachael Muschalek, Scott Herting, Grace Fletcher, and Bradley Due, for your advice, help with experiments, and support. I would especially like to thank Sarah Raines for her assistance performing the radial and dislocation force measurements of the devices. Her self-sufficiency, hard work, and dedication conducting those experiments was a tremendous help. Whether it was discussing the design of a project or winding down on a Friday night, each one of you made grad school and obtaining my PhD a better experience.

I would like to thank my parents, Roy and Karen Wierzbicki, as well as my sisters, Dana and Kate Wierzbicki, for their constant encouragement and support throughout my entire academic career. Grad school has been a difficult journey, and I couldn't have done it without you. I love you all.

CONTRIBUTORS AND FUNDING SOURCES

Contributors

This work was supported by a dissertation committee consisting of Professors Duncan Maitland, John Criscione, and Balakrishna Haridas of the Biomedical Engineering Department and Dr. Matthew W. Miller of the Texas Institute of Preclinical Studies.

Professor John Criscione was a valuable collaborator in analysis techniques and design of the radial force measurements in Chapter 4. Dr. Miller of the Texas Institute of Preclinical Studies provided valuable input in the design and requirements for the device. Additionally, he conducted the physiological *in vitro* deliveries in Chapter 2. Dr. Sonya Gordon of the Small Animal Clinical Sciences of Veterinary Medicine and Biomedical Sciences Department performed the physiological *in vitro* delivery experiments in Chapter 4, and provided valuable input on prototype performance. Dr. Ashley Saunders of the Small Animal Clinical Sciences of Veterinary Medicine and Biomedical Sciences Department and Scott Birch of The Center for Educational Technologies provided the physiological morphology CT datasets used to construct the silicone models used in Chapter 4. Professor Jefferey Raymond of the Department of Chemistry and Andrew Weems of the Department of Biomedical Engineering assisted in the method development and execution and evaluation of the DMA foam measurements in Chapter 3, respectively. Sarah Raines of the Electrical Engineering Department was a valuable collaborator throughout the completion of Chapters 3 & 4. She performed the dislocation and radial force measurements in Chapters 3 &4. Jesse Bryant of the Biomedical Engineering

Department conducted the removal force measurements in Chapter 2. Brandis Keller of the Biomedical Engineering Department collected scanning electron micrographs of the prototypes described in Chapter 4. Landon Nash of the Biomedical Engineering Department assisted in the development of the strut integrity testing protocol described in Chapter 4. Bradley Due of the Biomedical Engineering Department was a collaborator throughout the initial stages of Chapters 3 & 4. All other work conducted for the dissertation was completed by the student independently.

Funding Sources

This work was made possible in part by the National Institutes of Health/National Institute of Biomedical Imaging and Bioengineering Grant R01EB000462 and National Institutes of Health/National Institute of Neurological Disorders and Stroke Grant NS0899692.

NOMENCLATURE

Abbreviations:

PDA: Patent Ductus Arteriosus

MPA: Main Pulmonary Artery

MDD: Minimal Ductal Diameter

ACDO: Amplatz® Canine Ductal Occluder

ADO: Amplatzer™ Duct Occluder

AVP: Amplatzer™ Vascular Plug

SMP: Shape Memory Polymer

T_g: Glass Transition Temperature

DA: Ductus Arteriosus

ID: Inner Diameter

OD: Outer Diameter

NFC: Nitinol Foam Cage

SS: Stainless Steel

WA: Wide Ampulla

PDMS: Polydimethylsiloxane

CTA: Computed tomographic angiogram

PTFE: Polytetrafluoroethylene

TRF: Total Radial Force

HPED: N,N,N′,N′-tetrakis (2-hydroxypropyl)ethylenediamine

TEA: Triethanolamine

HDI: Hexamethylene Diisocyanate

TEMED: Tetramethylethylenediamine

APS: Ammonium Persulfate

NCO: Isocyanate

OH: Hydroxyl

SPB: Small Pore Bare

LPB: Large Pore Bare

PBS: Phosphate Buffered Saline

DMA: Dynamic Mechanical Analysis

SPC: Small Pore Clot

LPC: Large Pore Clot

Bis: Bis-acrylamide

SPH: Small Pore Hydrogel

LPH: Large Pore Hydrogel

ANOVA: Analysis of Variance

NFC_{Tn}: Thin walled NFC

NFC_{Tk}: Thick walled NFC

NFC_{TkEP}: Thick walled, Electropolished NFC

S_{ACDO}: ACDO Contact Pressure

s_{Tn}: NFC_{Tn} Strut Force

s_{Tk}: NFC_{Tk} Strut Force

B_{ACDO}: ACDO Blockwise Pressure

b_{Tn}: NFC_{Tn} Blockwise Force

b_{Tk}: NFC_{Tk} Blockwise Force

τ_{ACDO}: ACDO Wall Tension

τ_{Tn}: NFC_{Tn} Wall Tension

τ_{Tk}: NFC_{Tk} Wall Tension

TABLE OF CONTENTS

Page

LIST OF FIGURES

Page

LIST OF TABLES

Page

CHAPTER I

INTRODUCTION AND LITERATURE REVIEW

1.1 Characteristics of Canine Patent Ductus Arteriosus

Patent ductus arteriosus (PDA) is a congenital cardiovascular defect in which a normal fetal connection between the aorta and main pulmonary artery (MPA) does not close shortly after birth. This connection between the arteries leads to continuous left-to-right shunting of blood from the aorta to the MPA. The resulting overcirculation typically results in cardiac remodeling characterized by left ventricular and left atrial dilation with or without secondary mitral regurgitation. If uncorrected, the most common clinical outcome is left sided congestive heart failure or cardiogenic pulmonary edema and death [1, 2]. When left uncorrected, the one year mortality rate for this defect is reportedly 65% [3]. PDA accounts for 30% of all congenital defects found in dogs, making it the most common canine congenital heart defect [4].

PDA morphology is an important factor when determining the best closure method [5, 6]. It has been reported that morphology varies widely between dogs, and is not correlated with age or body weight [7]. Therefore, it is important to accurately measure the PDA dimensions prior to the procedure to ensure the best outcome. These measurements are usually carried out using angiography, transesophageal echocardiography, or both [8, 9]. Important factors to consider for device sizing include the minimal ductal diameter (MDD) and the ampulla shape, diameter, and length. The vessel between the aorta and MPA is known as the ductus, with the proximal (aortic side)

of the ductus being defined as the ampulla. The MDD is defined as the smallest diameter of the ductus as its connection to the MPA.

An investigation of PDA in 246 dogs revealed four characteristic PDA morphologies as shown in Figure 1.1 [7]. Type I PDA is characterized as a narrow tube that gradually tapers, less than 15 degrees, from the aorta to the MPA. Type IIA PDA is initially tube like, then abruptly narrows prior to the MPA. This narrowing is greater than a 50% reduction in ductal diameter. Type IIB PDA exhibits a taper (between 30-60 degrees), forming a conical shape, prior to an abrupt distal narrowing prior to MPA insertion. Type III PDA is tube-like with a relatively constant diameter (<20% ductal diameter reduction) [7].

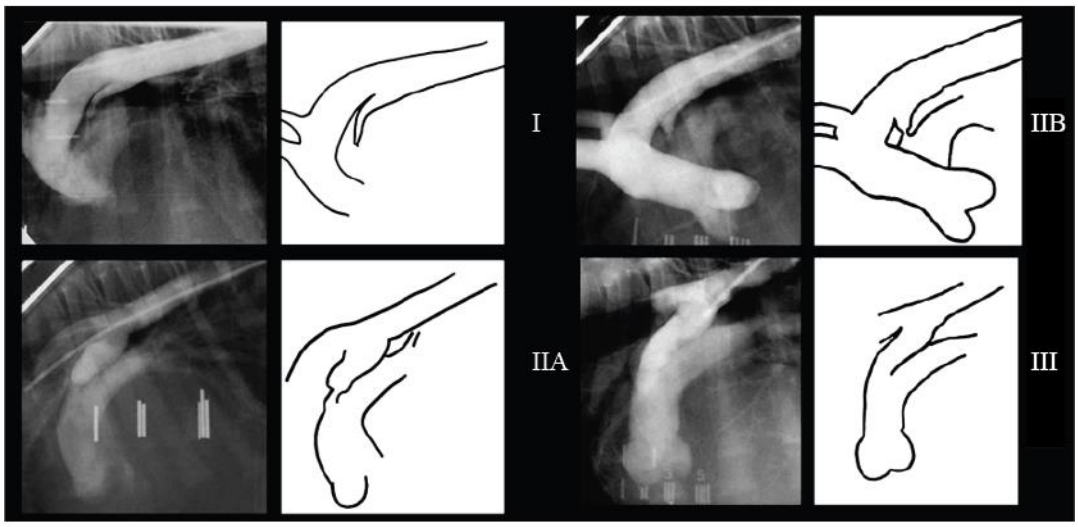

Figure 1.1: Typical PDA shapes. IIA and IIB are the most prevalent. Adapted from Miller et al [7]. Used with permission from Elsevier.

Type IIA PDA is the most common morphology, followed by Type IIB. Type III PDA is the least common morphology. Because it is usually larger in diameter than the other types, and the tube shape exhibits little taper (large MDD) to aid in securing a closure device, this type is usually treated via surgical ligation rather than through endovascular methods [7, 10].

In addition to identifying the PDA morphology, the PDA size greatly influences decisions related to method of closure [8, 9, 11]. Dimensions of interest include the MDD and the ampulla length and width. These dimensions are labeled in Figure 1.2 as A, B, and C respectively [8]. MDD dimensions (A) range from 1-9.5mm [7] but are more commonly seen between 2.2-3mm [7, 8]. Typical ampulla lengths (B) and widths (C) are 9 mm and 6-8 mm respectively [8, 12].

An important design consideration is the ability of the device to remain in position after deployment in the face of the large pressure gradient across the ductus from aorta to MPA. Physiological pressure gradients across the ductus have been measured using Doppler echocardiography as 80-140mmHg in conscious dogs [5, 13]. Following occlusion, the pressure gradient increases acutely and can exceed 200mmHg resulting in a reflex bradycardia, called the Branham reflex [14].

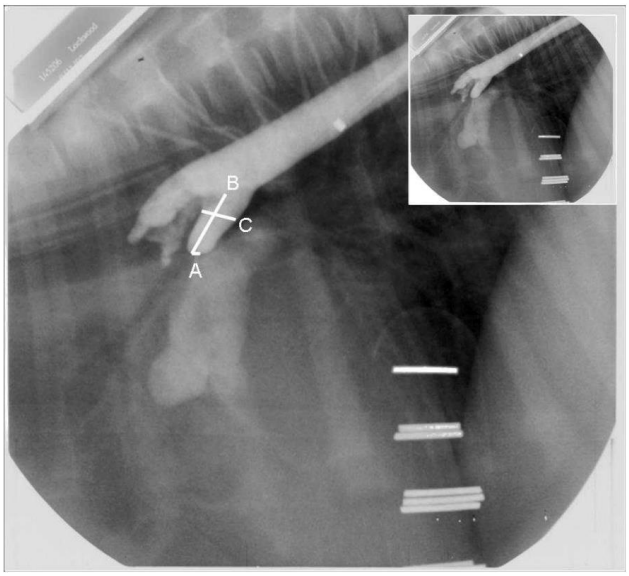

Figure 1.2: Typical PDA structures and dimensional measurements. A: Minimal ductal diameter (MDD). B: Ampulla length. C: Ampulla width [8]. Used with permission from John Wiley and Sons.

Following the procedure, there are multiple metrics used to determine success, chief being eliminating ductal flow (complete occlusion) or reducing residual flow to a hemodynamically insignificant volume. Occlusion is assessed 5-10 minutes immediately following deployment of the device via angiography and or transesophageal echocardiography. Additionally, an increase in diastolic blood pressure immediately following occlusion and the disappearance of pre-procedural continuous heart murmur indicates success. Finally, transthoracic echocardiography measurements to assess heart size and residual flow are performed at approximately 24 hours and six months post procedure. In rare cases, residual flow persists or develops at the 3-6 months reexamination, and if hemodynamically significant, can result in the need for a second procedure. [5, 15].

1.2 Current Devices and Treatment History

Historically, surgical ligation of the PDA via thoracotomy has been an effective method of PDA closure [1, 6]. However, PDA surgery suffers from the expected morbidity associated with a thoracotomy with a reported mortality rate of 0-11%[3, 16], and the risk of major non-lethal complications such as hemorrhage, pneumothorax, and chylothorax is 11-15% [16-19]. However, more recent publications suggest the mortality risk with surgical PDA ligation is on the lower side of the reported range, on average. Due to necessary morbidity and possible mortality, as in humans, in the dog, a viable minimally invasive treatment method is desired when available.

The first intravascular closure of PDA in the dog was reported in 1994 [20], and since this time, many studies have reported the viability of catheter delivered devices intended for PDA treatment in humans and canines [1, 11, 19, 21-26]. Transcatheter methods were initially investigated to reduce surgical trauma, and complications, as well as cost [6]. Current endovascular treatments include embolization coils, devices used to treat PDA in humans, and the Amplatz® Canine Ductal Occluder (ACDO).

1.2.1 Embolization Coils

Transcatheter embolization of PDA using embolic coils was the first commonly used endovascular closure technique of canine PDA [20]. Typical embolization coils (Figure 1.3) used for treatment include Gianturco or MReye® Flipper Detachable Embolization coils (Cook Medical) which are composed of surgical stainless steel coil windings and intertwined poly-Dacron fibers to enhance embolization [9, 11].

Figure 1.3: Fibered embolization coils intended for peripheral embolization in humans [9]. Used with permission from Elsevier.

Embolic coils are delivered either transarterially or transvenously [5] through a 4 or 6 Fr catheter [9]. To position the coils using the transarterial method, 1-1.5 coil loops are deployed into the pulmonary artery and the remaining coil is delivered within the ampulla [9, 11, 27], or the entire coil is delivered within the ampulla [5, 24]. To position the coils transvenously, most of the coil is deposited in the ampulla and 1-2 loops cross the MDD into the MPA [28, 29]. There are two methods used to release these coils during deployment: controlled release and free push. Controlled release coils allow for retraction of the device for repositioning or removal prior to release [9]. Examples of controlled release methods include a threaded release from the delivery cable and an interlocking release wire [25]. Free push coils are deployed by pushing the coil out of the catheter using a guidewire. There is reduced control with the free push coils due to the inability to retract the device, however, procedures can be carried out in smaller catheters compared to control release methods, allowing for the treatment of PDA in small dogs [9].

Three factors are considered when selecting the coil for treatment: coil wire gauge, coil loop diameter, and coil length. Embolic coils are available in various coil gauges (0.025”, 0.038”, 0.052”) and are used at different points during the procedure. It is recommended that the largest coil gauge that can pass through the catheter which has at least three revolutions when deployed be used for the initial coil [30]. This is followed by coils in a variety of diameters to seal leaks due to incomplete closure from previous coils. Smaller gauge coils are more compliant and better conform to the ductus [9]. The initial coil loop diameter used to occlude the ductus is usually chosen to be twice the diameter of the MDD and slightly larger than the ampulla width to secure the device in the ductus, followed by smaller sizes as needed [9]. Finally, the coil length determines the number of coils that can be used following complete deployment. A minimum of four loops is optimal for filling, and two to three coils are usually required to achieve complete occlusion in most dogs. An angiogram is recorded five to ten minutes after each coil delivered to assess residual ductal flow and the need to insert subsequent coils [9].

Immediately after completion of the procedure, 36-77% [5, 31] of dogs showed residual flow, however 85% of these cases resulted in complete occlusion upon follow-up at 3 months [11, 24, 31]. Less than 5% of those that did not show complete occlusion at follow up required a second procedure [9].

In addition to the positive outcomes, mortality rates of coil embolization procedures are low, 1%, compared to 3-8% during PDA surgical ligation [3, 16]. Other complications include coil migration and embolization to the lungs, which has been reported to occur in 13-22% of cases [5, 24]. Retrieval of these coils is not typically

attempted [11, 24] because adverse events have not been reported due the embolization of one or more coils [11, 24, 32]. However, coils cannot be used to close all PDA sizes and morphologies. As with all endovascular techniques, the PDA must taper sufficiently. Thus, the tube shaped (Type III) PDAs are not amenable to coil embolization because it does not adequately support the coils [9].

1.2.2 Devices for Humans (Amplatz® Ductal Occluder and Amplatz® Vascular Plug)

To simplify procedures and improve procedural outcomes compared to coils, devices intended for occlusion of human PDA have been investigated for use in dogs. These devices used to occlude PDA and vascular defects in humans were investigated to treat large PDAs, not amenable to coil embolization, and to achieve a more consistent occlusion [2, 5, 21, 22, 25]. Additionally, these devices are easier to deploy, reposition, and typically require less procedural time when compared to coils [2]. The two main devices investigated were the Amplatzer™ Ductal Occluder (ADO) (St. Jude Medical, St. Paul, MN) and the Amplatzer™ Vascular Plug (AVP) (St. Jude Medical, St. Paul, MN). The ADO (Figure 1.4, left) is designed to treat human PDA and the AVP (Figure 1.4, right) is used for correcting peripheral vascular defects in humans. The ADO consists of a nitinol frame with polyester fabric sutured to the frame to aid in occlusion. The AVP consists of a dense nitinol wire mesh which slows blood flow, resulting in occlusion.

Figure 1.4: Amplatzer™ ductal occluder (ADO), left. Amplatzer™ vascular plug (AVP), right. The ADO is indicated for human PDA closure and the AVP is indicated for human peripheral embolization [6]. Used with permission from Elsevier.

The ADO was designed specifically for transvenous deployment, the preferred approach in humans. It is delivered using a 5-7 Fr sheath [21, 22, 25]. The device is advanced through the femoral vein to the pulmonary artery, through the ductus, and into the aorta. The device is advanced until the distal retention disk is deployed. The retention disk is then pulled to lie against the aortic wall and then the sheath is then retracted to deploy the rest of the device within the ductus [21, 22]. After positioning of the device, the clinicians wait approximately 10-15 minutes to assess ductal occlusion. If occlusion is deemed satisfactory, the device is detached from the delivery cable via threaded release, and the delivery cable is retracted [22].

The AVP can be delivered transarterially or transvenously (transarterially is preferred in the dog) and requires a 4-6 Fr sheath, depending on the device size chosen to

occlude the PDA [2, 5, 25, 29]. The AVP is delivered within the ampulla of the PDA. Once stable positioning and adequate occlusion is confirmed, the device is released in a similar method to the ADO [25].

Two dimensions are considered when choosing the ADO device size, the retention disk outer diameter (OD) and the size of the plug [21, 22]. It is recommended that the retention disk be 20-30% larger than the diameter of the ductus and that the diameter at the base of the plug be 2 mm larger than the MDD [21, 22]. The retention disk, and outward pressure exerted by the plug prevents the device from sliding through the ductus into the pulmonary artery. When treating PDA with the AVP, the plug diameter is selected such that it is 30%-50% larger than the ampulla diameter [2, 5, 25].

Closure with the ADO resulted in complete angiographic occlusion in 65% of dogs immediately following device deployment and release. Follow-up showed complete occlusion in 75% of dogs at 24 hours, 89% at three months, and 95% at one-year. All documented residual flow was minimal and hemodynamically insignificant. In addition, transductal flow did not reappear in the dog once the PDA was documented to be completely occluded [22]. However, one study reported less favorable results, reporting only a 55% successful occlusion rate [6].

The occlusion outcomes of PDAs treated with the AVP were slightly less favorable than those treated with the ADO. Immediately post procedure, 47-50% were completely occluded [2, 5, 26]. Follow up at 24 hrs showed complete occlusion in 61-76% of cases, and 66% at three months [2, 5, 26].

Complications using the ADO included severe intra procedural arrhythmias, which could be due to the transvenous approach required for delivery of this device, necessitating the sheath be advanced through the right heart. Sission et al reported two deaths, which were believed to be a result of arrhythmias and atrial fibrillation [21, 22]. Complications were more prevalent when using the AVP compared to the ADO. When the ampulla dilates, shortly after occlusion, the AVP can begin to rotate and migrate from the desired position, greatly increasing the flow through the ductus [5, 25]. Additionally, while simpler to deliver than coils, disadvantages to this include the large sheath required to deliver this device. Many dogs cannot be treated due to inadequate femoral artery size.

1.2.3 Amplatz® Canine Ductal Occluder (ACDO)

The Amplatz® Canine Ductal Occluder (ACDO) (Infiniti Medical, LLC, Menlo Park, CA) was specifically designed to treat canine PDA and conform to the canine PDA morphology [33]. Like the AVP and ADO, this device utilizes a dense self-expanding nitinol mesh to occlude the ductus [33]. This device was specifically developed by Nguyenba et al in conjunction with a company to address issues associated with other catheter treatment methods, such as, ease of deployment, device migration, and completeness of occlusion [1, 33]. The device, shown in Figure 1.5 consists of a distal disk, used for positioning against the MPA ostium, within the MPA, a narrow portion (waist) which is placed across the MDD, and a proximal disk that is deployed within the PDA ampulla that helps stabilize the device within the PDA.

The ACDO is delivered transarterially, from the femoral artery, using either a 4-9 Fr sheath, or 6-9 Fr guiding catheter [33]. It has been reported that dogs greater than 3 kg can be treated with this device (4 Fr sheath) [33]. When delivering the device, the ACDO is advanced through the sheath/catheter to the MPA, the device is advanced out of the catheter until the distal disk is protrudes into the MPA. The device and catheter are then retracted until the disk contacts the MPA ostium of the ductus. The sheath is then retracted, while holding the delivery wire stable, to fully unsheath the ACDO. The PDA is then inspected for adequate occlusion prior to release, and if deemed acceptable, the delivery cable is rotated counter-clockwise, and the device is released from the delivery wire [33].

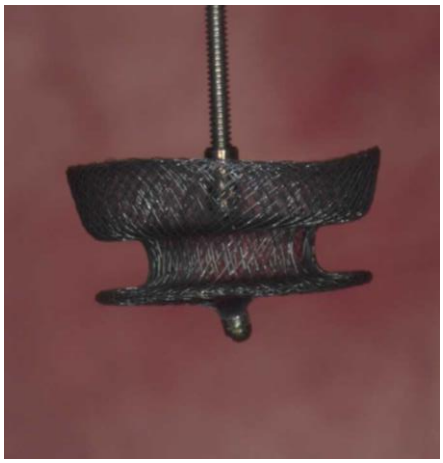

Figure 1.5: Amplatz® canine ductal occluder (ACDO). The ACDO was specifically designed to conform to and occlude canine PDA.

The ACDO is available in a variety of sizes with the waist diameter ranging from 3-10 mm in 1 mm increments and in 12 and 14 mm. These allow for the treatment of many different PDA sizes. Sizing is determined by the MDD. The device size is selected such that the waist is 1.5-2.7x larger than the MDD, the recommended target is 2x MDD in most cases [1, 5, 15, 33].

Clinical studies have shown this device to be very effective at occluding PDA. Immediately post-procedure, 75%-94% have complete occlusion, and at 24 hours, 97-100% of PDAs were fully occluded [1, 5, 15]. There was no evidence of the reappearance of ductal flow in any ductus demonstrated to be completely occluded (recanalization) at three months post procedure [1].

Complication rates when using this device are low. Device related complications have been reported as 3-6% [1, 5, 15]. These complications were either due to user error [15], improper device sizing [1, 5], or device migration into the pulmonary artery, likely a consequence of the first two [1]. In the case of improper device sizing, the device was retracted into the sheath/catheter and removed and a second more appropriate sized (smaller or bigger as required) device was delivered successfully. A smaller device is selected if the deployed device doesn't assume an acceptable shape and a larger device is selected if the push-pull test results in easy dislodgement into the MPA. In one study, there were no significant clinical complications that resulted in the devices that embolized in the pulmonary artery [1], however, antidotal persona commination with Drs. Miller and Gordon confirm that this is a rare complication and as with MPA coil embolization is often non-fatal and does not require retrieval [12].

1.2.4 Summary of PDA Occlusion Methods

All transvenous PDA occlusion methods in the dog described above have been determined safe to use and have an overall success rate (including some clinically insignificant residual flow in some dogs) of 92% [5]. However, when comparing occlusion devices, the ACDO performed the best, occluding 98-100% of dogs [1, 5, 15], followed by AVP (93-100%) [2, 5, 26], ADO (89-100%) [22], and coils (86-100%) [5, 11, 22, 24, 28, 29]. It is recommended that different PDA morphologies and sizes may require different endovascular techniques and devices [7, 21]. Type III PDA is the most difficult to occlude using currently available devices due to the lack of taper at the pulmonic ostium. However, the ACDO has been reported to successfully occlude Type III morphologies in some dogs [1, 6]. The AVP and coils are not recommended for use in Type III PDAs and coils should not be used in PDAs with MDDs greater than 5 mm due to the higher risk of migration into the MPA [21], the ACDO has been successfully deployed in wide range of MDDs and a variety of morphologies, including Type III [1, 6]. Use of the ADO has been reported in older dogs with large ducti [6]. To date, there are no published guidelines for method (surgery versus device) or device selection in dogs with PDA, and as such, is based on clinician preferences, availability of experienced individuals (veterinary cardiologists and surgeons), and to some extent, cost and patient size.

It is important for the device to remain in position once deployed. Coil migration is relatively common and is reported to occur in 22% of cases [24], whereas this occurs in 0-6% of cases when the PDA is treated with the ACDO [1, 5, 15]. Additionally, migration

has been reported with use of the AVP such that the AVP can become disengaged from the ampulla and migrate into the MPA after delivery [2].

The ACDO, AVP and ADO all require relatively large delivery systems, ranging from 4-9 Fr sheaths. Additionally, the ADO delivery system has been reported to kink during delivery due to the sharp bends required for the transvenous delivery and has been assessed as a poor treatment method, especially for dogs under 5 kg [6]. While coils are not ideal or most reliable method to treat PDA, they still offer the smallest delivery system, down to 3 Fr catheter [23], and many dogs must be treated with coils due to this sizing constraint [5, 33].

While historically less invasive than surgical closure, device closure procedures can cost as much or exceed the surgical ligation cost, making many of these procedures cost prohibitive to dog owners [10]. However, despite the high cost and large delivery system required, the ACDO has been shown to exhibit better occlusion, lower complication rates, and is becoming preferred over the other endovascular closure methods [5].

1.3 Device Improvements Using Shape Memory Polymers

Unlike the current devices used to treat PDA which use a dense nitinol wire mesh or coils with embolic fibers, we plan to utilize shape memory polymer (SMP) urethane foams to occlude the ductus. Shape memory polymers are a class of materials which can be deformed, set into a temporary configuration, and actuated via an external stimulus, such as heat, to recover their original configuration [34, 35]. When an SMP is heated above

its glass transition temperature (T_g), it enters its rubbery phase and can be easily deformed. Above T_g, the amorphous chains of the polymer can be elastically deformed reducing the entropy of the system. If the SMP is held in a deformed configuration and cooled below its T_g, the chains will be fixed in the deformed shape. When the SMP is heated above its T_g, the chains will relax to their original configuration and the polymer will regain the entropy lost during deformation [35].

Shape memory polymer foams hold excellent promise in the biomedical device field. The unique compression and recovery capabilities of the material make them amenable to endovascular device deliveries. Singhal et al. have presented ultra-low density SMP foams exhibiting 70x volume expansion and 97-98% shape recovery. Additionally, the foams exhibit sharp, tailorable T_g's between 45-70°C, allowing the user to choose the best composition for their desired application [36]. The foams have also displayed excellent biocompatibility *in vitro* and *in vivo* [5, 37, 38]. Rodriguez et al. performed a study analyzing the ninety-day biocompatibility of SMP foams in pigs, which showed stable thrombosis and cell infiltration in the foam volume, and less inflammatory response compared to an FDA approved suture material, indicating excellent biocompatibility and healing [37, 38].

The interesting properties of these foams have prompted investigation for use as potential embolic agents for endovascular occlusion [39, 40]. In contrast to the current devices which utilize a dense wire mesh to occlude flow, we plan to occlude the ductus using SMP foam.

1.4 PDA Design Criteria

Our primary consultant for this device was Dr. Matthew W. Miller, a board certified veterinary cardiologist with the Texas A&M Institute for Preclinical Studies. Through our meetings and literature review, we've determined five criteria that must be considered to develop a competitive device: Retraction, occlusion, detachment, device/delivery size, and radiopacity. The design criteria are summarized in Table 1.1 below.

Device retraction is defined by the ability to retrieve a device from the PDA once fully advanced outside the catheter, when still attached to the delivery cable. Device reposition is defined as the ability to fully advance the device outside the catheter, retrieve the device into the catheter, and redeliver the device to the site at a more ideal position. The devices currently used to treat PDA are repositionable, excluding free push coils, therefore, our device must be at least retractable for the design to be competitive. However, it was advised that the device does not need to be repositionable. This is an attractive characteristic, but it is not required for the end device.

The device must occlude the vessel and promote local clot formation to ensure that the PDA is blocked. Polyurethane shape memory polymer foams will be used to occlude the vessel as the foam has been shown previously to embolize and exhibit healing *in vivo* and *in vitro* [36-38]. The ACDO exhibits clotting in approximately ten minutes [15]. The proposed device should match this metric for easier device adoption. However, Dr. Miller advised that a fast clotting time is not an important factor, if the device remains in position while the clot is forming, and the clot is not needed to hold the device in position.

The device will require a simple to operate, inexpensive to manufacture, detachment mechanism to release the device from the delivery wire. The ACDO utilizes a microscrew mechanism to detach from the delivery wire.

To maximize the number of animals that can be treated with this device, the prototype must be deliverable through a 4 Fr sheath or smaller. This sized sheath can be properly positioned in most dogs with PDA. Using any catheters or sheaths larger than 4 Fr removes a subset of dogs that can be treated with the device as it will not fit through the femoral artery. Delivery within a 4Fr catheter would be ideal, but is not required.

Finally, the device must be radiopaque and visible under fluoroscopy to facilitate optimal positioning by the physician.

Table 1.1: Summary of design requirements.

Design Criteria	Design Requirement
Device Retraction Reposition	Must be retractable. Does not have to be repositionable Must be retractable or not a viable option
Occlusion	Does not have to occlude immediately, but device must remain in position
Detachment	Should have a simple, inexpensive detachment mechanism
Delivery Mechanism	Most PDA's accessible with 4Fr sheath 4Fr catheter would be ideal, but not required
Radiopacity	Must be visible under fluoroscopy

CHAPTER II

MECHANICAL AND IN VITRO EVALUATION OF AN EXPERIMENTAL CANINE PATENT DUCTUS ARTERIOSUS OCCLUSION DEVICE[*]

2.1 Introduction

The ductus arteriosus (DA) is a normal fetal connection between the aorta and main pulmonary artery (MPA). During the fetal development, the function of the DA is to shunt blood flow around the developing, but uninflated lungs. It remains open during development due to low oxygen tension [41] and the circulation of vasodilators [42-44]. After birth, oxygen tension greatly increases and the production of vasodilators decreases, causing the DA to constrict and close [45, 46].

However, in some cases, the DA does not close, resulting in a condition known as patent ductus arteriosus (PDA). The residual communication between the two arteries leads to continuous left-to-right shunting of blood between the descending aorta to the MPA. This loading can result in substantive cardiac remodeling and numerous clinical manifestations including cardiac arrhythmias, congestive heart failure, ventricular dilation, mitral valve regurgitation, pulmonary over-circulation, and death [1, 2]. This defect affects 6.8 in 1000 canine births accounting for 28% of all congenital cardiac malformations, making it the most common congenital cardiac defect found in dogs [4].

[*] Reprinted from Journal of the Mechanical Behavior of Biomedical Materials, Vol 59, MA Wierzbicki, J Bryant, MW Miller, B Keller, DJ Maitland, "Mechanical and in vitro evaluation of an experimental canine patent ductus arteriosus occlusion device," pgs 156-167, Copyright 2016, with permission from Elsevier.

When left uncorrected, the one-year mortality rate for this defect is 65% [3], necessitating closure.

Traditionally, surgical ligation of the PDA via thoracotomy has been the accepted treatment for PDA in canines [1, 3, 47, 48]. However, this highly invasive surgery results in operative mortality rates from 0-11% [3, 16-19, 47] and risks of major complications such as nonfatal hemorrhage, pneumothorax, and chylothorax are 11-15% [16-19], increases the appeal of a viable minimally invasive treatment method [6].

The first intravascular treatment of PDA in the dog was reported in 1994 [20]. Since this initial report there have been studies investigating the viability of treating canine PDA with endovascular delivered occlusion devices intended for human use, such as embolization coils, the Amplatzer™ Vascular Plug (AVP), and the Amplatzer™ Ductal Occluder (ADO). While these had varying success, there were still issues present such as, completeness of occlusion, device migration, delivery system size, and ease of delivery [2, 5, 6, 9, 21, 22, 24, 25, 27].

The Amplatz® Canine Ductal Occluder (ACDO) (Infiniti Medical, LLC, Menlo Park, CA), designed to address limitations of other endovascular treatments, was the first device designed to specifically conform to the canine PDA morphology [1, 33] and is currently the most widely used device to close PDA in dogs. The device is a dense, self-expanding nickel titanium (nitinol) mesh which consists of a distal disk, used for positioning against the MPA ostium, a narrow waist which is placed within the minimal ductal diameter (MDD), and a proximal, cupped disk that helps stabilize the device within the PDA [33]. Clinical studies have shown the ACDO to be very effective at occluding

PDA, with 70-75% showing complete occlusion acutely upon implantation and up to 97-100% at 24hrs [1, 5, 15]. However, while effective, this device is very expensive and cost prohibitive to some dog owners, pushing the cost of transvascular occlusion to approach and even exceed the cost of surgical ligation. Additionally, the size of the delivery system necessary for large ACDO's can reduce the number of patients that can be treated with this device [15]. Canine PDA size is not associated with age or body weight [7], therefore, a small dog (<4 kg) may have a large PDA that cannot be treated because of the large delivery system required [6]. Therefore, there is a clinical need to develop a device addressing these issues.

A prototype device which utilizes shape memory polymer (SMP) urethane foams has been developed for endovascular PDA treatment. Shape memory polymers are a class of material which can be heated above a characteristic glass transition temperature (T_g), deformed, cooled below the T_g setting it into a temporary shape, and actuated by increasing the polymer's temperature above the T_g via an external stimulus, such as heat, to return to their original shape [35]. These materials have been proposed for several biomedical device applications including use as embolic agents for endovascular occlusion [39, 40]. The ability of the foam to be delivered, compressed, and actuated to its original volume lends itself well to endovascular device delivery. Singhal et al. have demonstrated ultra-low density SMP foams with up to 70x volume expansion, 97-98% shape recovery after multiple cycles, and sharp, tailorable transition temperatures between 45-70°C [36]. In addition, the foams have shown excellent biocompatibility *in vitro* and

in vivo, exhibiting the recruitment of collagen and connective tissue to form stable scar tissue, as well as clot formation within two minutes[36-38, 49].

The goal of the present research is to develop an effective prototype PDA occlusion device with an equal or lower profile delivery system and with a lower cost than the ACDO. Decreasing the delivery profile of both small and large devices will allow clinicians to treat a greater population of dogs using minimally invasive techniques. Secondly, as the ACDO has become cost prohibitive, we have attempted to minimize the cost through reduction of materials used.

For the device to be successful, it must conform to multiple design requirements, including that the device must: be retractable back into the catheter/sheath after delivery, be deliverable through a 4Fr sheath with 1.3mm inner diameter (ID) or smaller, occlude/reduce flow through the PDA to hemodynamically insignificant levels [36, 50], remain stable and not migrate once placed into the PDA, and be visible under fluoroscopy. These criteria will be evaluated in multiple mechanical and *in vitro* studies, which include radial pressure and removal force measurements, device stability and flow reduction measurements at physiological and elevated pressure gradients, and delivery into a physiologically representative model under fluoroscopy. Additionally, the mechanical properties and characteristics of the prototype device were compared to the properties of the ACDO.

2.2 Methods

PDA occlusion prototypes were fabricated using a custom process and then evaluated with mechanical and *in vitro* benchtop studies. Experiments performed included measuring the radial pressure the devices imparted on the vessel wall, measuring the force required to remove the device once positioned within the ductus, and evaluating device stability when subjected to physiological and elevated pressure gradients in simplified and physiologically representative *in vitro* models. These methods enable evaluation of the efficacy of the current prototype and how to approach further development of this design.

2.2.1 Device Fabrication

A monolithic nitinol foam cage (NFC), composed of a self-expanding nitinol frame and an SMP foam, was manufactured by laser cutting slots into a thin walled nitinol tube (NDC Inc, Fremont, CA) using a 248nm excimer laser (Resonetics, Nashua, NH) outputting approximately 100mW of power. The part was then deburred using abrasive paper and sonicated in isopropyl alcohol, followed by a heat treatment process to set the shape.

The shaping process is detailed in Figure 2.1. First, stainless steel (SS) collars are positioned over the struts to prevent fracture formation during strut expansion, and a gauge pin was placed within the lumen of the tube to keep the device axial during the compression process, shown in Figure 2.1A. A SS spacer was placed inside the unexpanded proximal struts to aid in the shaping of the rectangular geometry as shown in Figure 2.1B, and positioned onto the fixture. The device was compressed axially to expand

the proximal (Figure 2.1C) and distal cages (Figure 2.1D); an external frame restrained the proximal cage, setting its shape. The device and fixture was then heat treated at 550°C for seven minutes in a furnace and subsequently quenched in room temperature water.

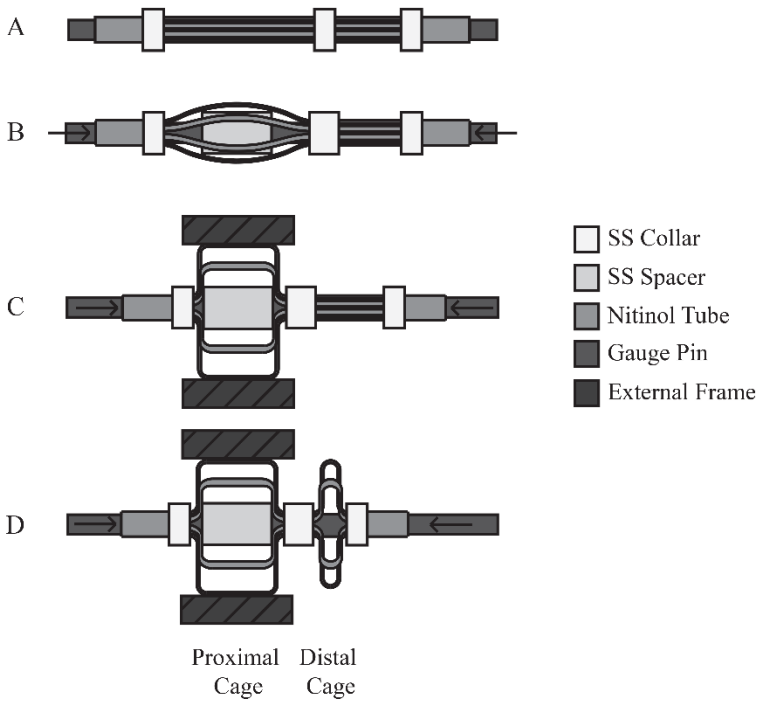

Figure 2.1: NFC shape setting procedure. A: Laser cut nitinol tubing with SS spacers positioned and gauge pin placed within lumen. B: Interior SS spacer positioned in proximal struts. C: Tube is compressed axially so proximal cage opens. D: Tube is compressed axially further to expand distal struts.

After the frame was created, a threaded detachment SS tube and nitinol backbone wire were attached. The backbone, constructed using 0.010" nitinol wire (NDC Inc, Fremont, CA) welded to a SS hypotube, was laser welded to the lumen of the threaded

detachment tube using an iWeld 990 (LaserStar, Riverside, RI), and this assembly was laser welded within the proximal lumen of the nitinol device frame.

The SMP foam composition used in these devices was the 0TM composition described and synthesized in a similar way to those reported by Singhal et al. (Singhal et al., 2013). These foams were chosen for their rapid expansion in water (~2min in 37°C water) [51] allowing for fast occlusion of the PDA ductus, similar to the occlusion times of the ACDO (5-20 minutes) [15, 36]. These foams were post processed following the protocol described by Hasan et al. [52]. Foam cylinders 6mm diameter and 4mm long were cut from the cleaned foams using surgical biopsy punches and crimped over 0.010" nitinol wire using a radial crimping head (Machine Solutions, Flagstaff, AZ) to a diameter less than the nitinol tube inner diameter (ID). The compressed foams were threaded from the nitinol wire onto the device backbone wire within the proximal cage. Figure 2.2 shows a comparison of the ACDO to the NFC.

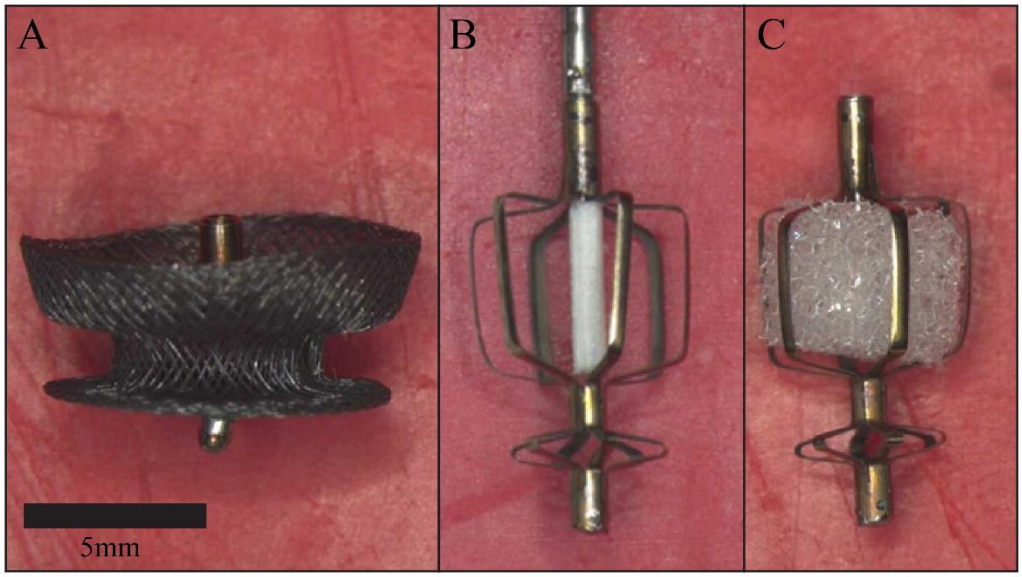

Figure 2.2: PDA device comparison. A: 6 mm ACDO (sized at the device waist); B: NFC, foam compressed; C: NFC foam expanded. (Same scale across frames).

2.2.2 Model Fabrication

Four different models were constructed for device testing based upon PDA geometric classification as described in Miller et al. [7]. These included three simplified models (IIA, IIB, and wide ampulla (WA) taper), and a physiologically representative model of canine PDA. The dimensions and shapes of the simplified models are shown in Figure 2.3 and are based upon published data reported in Miller et al. [7]. The IIA and IIB models emulate the most common types of canine PDA morphology, and the WA model, based upon the IIA taper, was used to evaluate device performance when the device struts did not contact the vessel wall due to ampulla, the portion of the ductus proximal to the MDD, expansion [2, 7, 8].

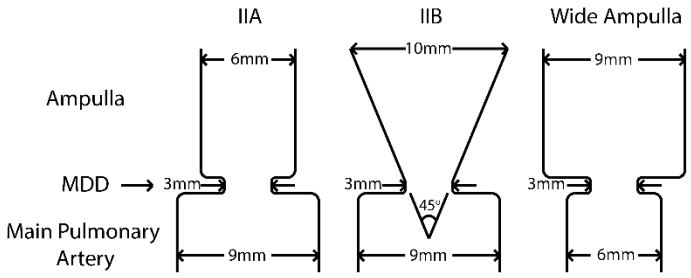

Figure 2.3: Simplified PDA model geometries. Dimensions and shapes based upon common canine PDA shapes [7].

Simplified PDA models were created by 3D printing the PDA geometries, casting polydimethylsiloxane (PDMS) around the 3D printed model, and dissolving the printed material, leaving the vessel geometry.

The physiologically representative vessel geometry was modeled using a computed tomographic angiogram (CTA) of a canine PDA. The surfaces of the descending aorta and MPA were extracted and sectioned using a trial version of Amira 3D analysis software (FEI Visualization Sciences Group Burlington, MA). Because the CTA provided was an unusual morphology, the geometry was modified to resemble a more typical IIA taper. The extracted volume was then imported into Solidworks (Dassault Systemes, Waltham, MA) for further processing and manufactured in a similar manner to the simplified PDA models using PDMS.

2.2.3 Radial Pressure

Radial pressure applied to the vessel wall by the device was measured to ensure that the device would not impose severe vessel trauma or ampulla rupture. Experiments

were performed using an Instron 5965 Test Frame (Instron, Norwood, MA) and Blockwise RJA62 J-Crimp^{TM} Radial Compression Station (Blockwise Engineering LLC, Tempe, AZ), as shown in Figures 2.4A and 2.4B. The Blockwise employs a linear relationship between the positions of the extension arm and the diameter of the compression station shown below as,

$$\Delta D = 0.7374 \cdot \Delta x, \tag{2.1}$$

where *ΔD* is the change in diameter and *Δx* is the change in vertical position, and between the measured load seen by the extension arm and the radial force exerted by the device as,

$$TRF = 2.712 \cdot F, \tag{2.2}$$

where *TRF* is the total radial force and *F* is the force measured by the load cell. The *TRF* can be converted to radial pressure using,

$$P = \frac{TRF}{Strut\ SA}, \tag{2.3}$$

where *Strut SA* is the surface area of the struts in contact with the Blockwise. To estimate the surface area of the ACDO in contact with the vessel wall, the ACDO was placed on a uniaxial tensile tester and elongated such that the diameter of the elongated ACDO was approximately the same as the vessel diameter to be tested. Images were captured and length measurements were conducted using ImageJ software (NIH, Bethesda, Maryland). These measurements were then used to estimate the surface area.

The radial pressure of the NFC and a 6mm ACDO (sized at the device waist) was measured at five different diameters, 3.3, 4, 5, 5.5, and 6mm, to simulate the device being deployed in different sized vessels. Prior to each run, the 50 N load cell was balanced. A baseline measurement was recorded for each diameter and was subtracted from each data

set. Force measurements were recorded at a rate of 10 Hz for 30 s. Three NFC devices were tested at each diameter, and each test was conducted at least three times for each device. A single ACDO was tested at least three times at each diameter. The distal cage/disk of the NFC devices and ACDO was constrained during each of these tests with a Teflon tube, (Figure 2.4C), allowing only the proximal cage to expand, because it would not exert force on vessel walls radially *in vivo.*

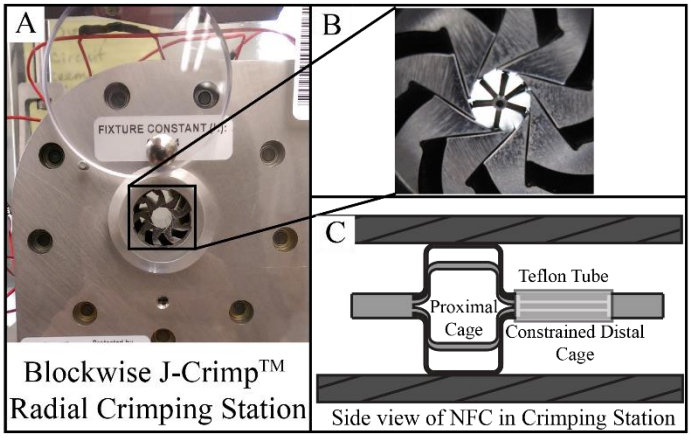

Figure 2.4: Radial pressure testing setup. A: Blockwise RJA62 J-Crimp™ radial compression station attached to Instron test frame. B: Enlarged, front view of compression blades, set to 5 mm diameter, with NFC deployed. C: Side view schematic of deployed NFC within compression station showing constrained distal cage.

The radial pressure exerted by the devices was compared to the estimated burst pressure of the PDA vessel calculated using,

$$P = \frac{2st}{d_0}, \tag{2.4}$$

where P is radial pressure, s is the ultimate material strength, t is wall thickness, and d_0 is outer diameter of the vessel. From this method, the approximate burst pressure of the canine aorta was calculated as 200kPa (1500mmHg) [53, 54].

2.2.4 Removal Force

Experiments measuring the removal force were carried out using an MTS Synergie 400 tensile tester (MTS, Eden Prairie, MN). During experimentation, the devices were deployed into simplified PDA models and submerged within an isothermal water bath held at 37-38°C. The distal end of each device was attached to the MTS gripper and was extended at 2.5mm/min until it was pulled through the MDD. Force was recorded at a rate of 10Hz. Three NFC devices and an ACDO were tested in each simplified PDA geometry. To assess repeatability, each NFC device frame was tested using three different foams (each 6mm diameter x 4mm long) as the foam is removable from the nitinol frame. The ACDO device was tested in each geometry at least three times. The removal force was recorded as the force required to dislodge the device from its implanted position, such that the proximal cage/disk protruded into the MPA.

2.2.5 Device Stability and Flow Reduction in Simplified in vitro Models

The goal of this test was to determine whether the NFC device could withstand physiological and elevated pressure gradients and the amount of device migration and flow reduction when positioned into the previously described simplified PDA models.

2.2.5.1 Flow Setup

A flow system was constructed and a representative schematic is shown in Figure 2.5. Pressure gauges were placed proximally and distally to the PDA models to allow for measurement of the pressure gradient across the device. A water bath was used to hold the flow loop at 38°C, emulating the canine body temperature [55]. To control the pressure gradient across the ductus, a Y connector was placed prior to the PDA and a bypass arm was added. By adjusting the flow rate of the pump, the pressure gradient across the device could be controlled. A hemostasis valve was used to introduce the delivery sheath into the flow loop to the model geometry.

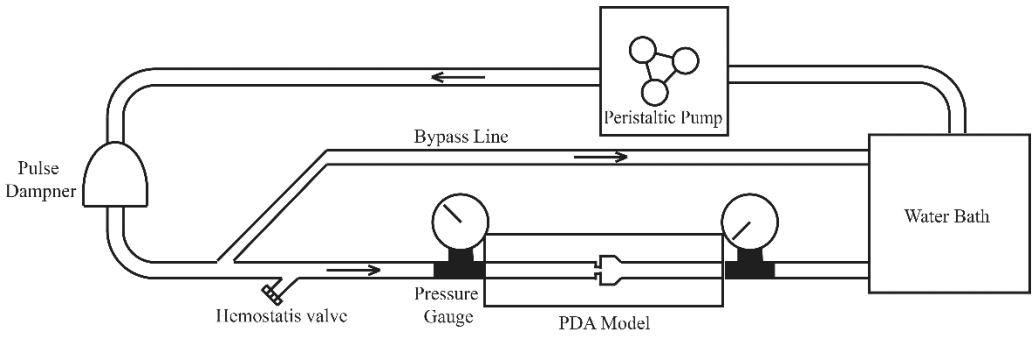

Figure 2.5: Schematic of flow loop used for *in vitro* testing.

2.2.5.2 Device Preparation and Delivery

NFC devices were prepared with compressed, 6mm wide, 4mm long foams prior to experimentation. NFC and ACDO devices were delivered through a 4Fr sheath (Cook Medical, Bloomington, IN). The sheath was advanced through the ductus and the device's

distal cage was deployed under a no flow condition. The sheath was then retracted such that the distal cage was then in contact with the modeled pulmonic ostium of the ductus. The proximal cage was then unsheathed, deploying the device. After the device was fully advanced out of the sheath, the delivery cable was rotated counter-clockwise to unscrew the cable from the device. Following release, the sheath and delivery cable were retracted out of the flow loop and the foam was allowed to fully expand.

2.2.5.3 Device Stability Tests

Once the device was positioned and foam expanded (~1-5mins), the pump was turned on and the flow rate was set such that the pressure gradient across the PDA was approximately 100mmHg (13.3kPa) corresponding to the typical physiological pressure gradient across the ductus [5, 13]. The flow rate was then held constant and images of the device and the pressure gradient were recorded every minute for five minutes. Following the test at 100mmHg, the flow rate from the PDA arm of the flow loop was measured. Following the flow measurement, the systemic flow rate was increased to obtain a pressure gradient across the ductus of approximately 300mmHg (40 kPa) to act as a safety factor, and the image and flow rate collection procedure described above was completed. After collection of the final flow rate, the device was removed and the un-occluded flow rate was collected for the flow speed used at each pressure gradient. Three different NFC devices were used and subjected to these tests three times in each of the PDA models for a total of twenty-seven tests. One 6mm ACDO was tested three times in

each of the PDA models. The ACDO was only evaluated at the physiological pressure gradient.

Following the tests, device migration was assessed by measuring the length the distal end of the device moved relative to the MPA wall at zero (baseline), five (100 mmHg), and ten minutes (300 mmHg) by importing the collected images into ImageJ image analysis software.

2.2.6 Physiological Model in vitro Experimental Setup

An *in vitro* test was conducted within the Texas Institute of Preclinical Studies (TIPS) facility at Texas A&M with the goal of obtaining clinician feedback regarding the ease of delivery/use of the NFC compared to the ACDO when deployed into a physiologically representative model under fluoroscopy. The primary tests that were conducted included evaluating device stability, retractability, and flow reduction.

2.2.6.1 Device Preparation

Four NFC devices and a 6 mm ACDO device were used in this experiment. Table 2.1 below describes the device variants used.

Table 2.1: Physiological *in vitro* device list. Specifications of devices used in the physiological *in vitro* tests.

ID	Device Variant	Expanded Foam Diameter
NFC 1	4.5mm OD distal cage	6mm foam
NFC 2	4.5mm OD distal cage	8mm foam
NFC 3	6mm OD distal cage	6mm foam
NFC 4	4.5mm OD distal cage	6mm tungsten-doped foam (Rodriguez et al., 2012)
ACDO	N/A	6mm waist (designed to occlude 3mm MDD)

The 4.5 mm OD distal cage type NFC design was tested in the simplified *in vitro* studies, and the 6 mm OD distal cage design was a variation used to test its ease of delivery when positioning compared to the smaller distal cage devices. The different sized foams were tested to monitor how foam diameter influenced flow reduction. The tungsten-doped foam device was tested to evaluate visibility under fluoroscopy compared to the non-radiopaque foams [37].

2.2.6.2 Device Delivery

The same flow loop used for device stability measurements in Section 2.5.1 was used for these tests. Devices (Table 2.1) were preloaded into polytetrafluoroethylene (PTFE) tube introducers and loaded through a check-flow valve at the end of the 4Fr sheath by a veterinary cardiologist (Dr. Matthew W. Miller) and advanced to the model geometry under fluoroscopic guidance. Devices were deployed in a similar manner as

described in Section 2.5.2. Following deployment, the pressure gradient across the device was increased to 100mmHg (13.3 kPa) by increasing the systemic flow rate and radiographic contrast was injected into the flow loop to qualitatively assess flow reduction. Additionally, when NFC 4 was implanted, the pressure gradient was increased to 200mmHg (26.7 kPa), which can occur acutely, and contrast was injected to evaluate flow reduction.

2.2.6.3 Device Retraction

Device retraction was performed on NFC 3 by the physician by pulling on the delivery cable to recapture the delivered device into the sheath.

2.3 Results

2.3.1 Radial Pressure

The average radial pressure exerted by each device at each diameter is shown in Figure 2.6. Radial pressure for the ACDO and NFC decreased as the ampulla diameter increased. The pressure exerted on the wall by the ACDO was approximately equal to that of the NFC at ampulla diameters smaller than 5mm, but was higher at ampulla diameters of 5.5 mm and 6 mm. The peak pressure exerted on the wall by the ACDO was 36kPa (270 mmHg). The peak pressure exerted by the NFC was 33 kPa (247 mmHg). All NFC and ACDO devices tested exerted pressures below the calculated canine aorta burst pressure of 200 kPa (1500 mmHg).

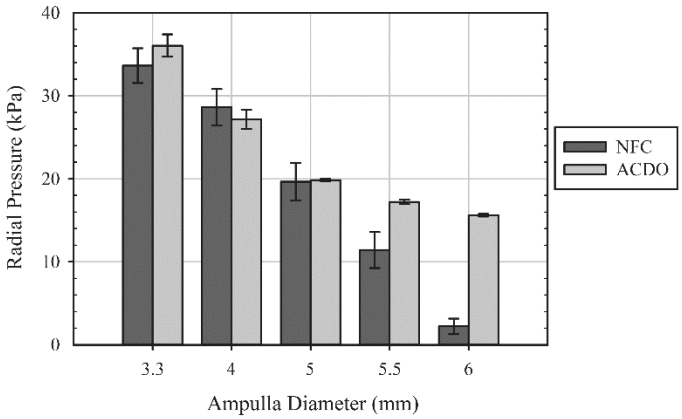

Figure 2.6: Average radial pressure. Average radial pressure of the NFC compared to the ACDO at each ampulla ID tested.

2.3.2 Removal Force

Figure 2.7 shows the average removal force of the NFC and ACDO devices in each of the three simplified PDA geometries tested. The average removal force of the ACDO was higher than that of the NFC across all geometries tested. The average removal force was lowest for both the NFC and ACDO in the IIB geometry. The removal force of the NFC in the wide ampulla model was similar to that of the IIA model.

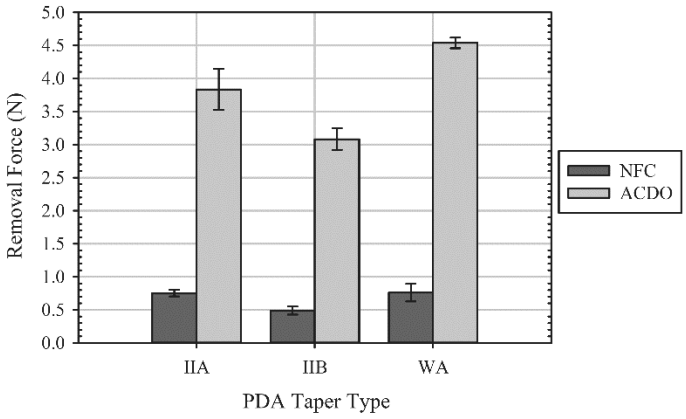

Figure 2.7: Average removal force. Average removal force of the NFC and ACDO for each simplified vessel geometry.

2.3.3 Simplified in vitro Testing

2.3.3.1 Device Stability

Figure 2.8 shows representative images of the devices after deployment in the *in vitro* benchtop studies, after five minutes at 100mmHg, and after five minutes held at 300mmHg. The average migration was measured and calculated at these time points and is shown in Table 2.2. There was additional migration after the pressure gradient was increased to 300mmHg. The ACDO did not exhibit observable migration in any models tested.

The devices in the IIA taper exhibited the most axial migration (Figure 2.8A). The proximal cages would slide in the ampulla when subjected to physiological pressures before contacting the MDD taper. The devices would slightly rotate in the IIB model at the elevated pressure gradient as shown in Figure 2.8B. The devices remained in position relatively well at the 100mmHg pressure gradient (B.2), but would slip and the device

would slightly rotate at the 300mmHg pressure gradient (B.3). The lowest migration was seen in the wide ampulla model (Figure 2.8C). The struts were fully deployed and rested on the flat MDD taper. The devices remained in position in the ampulla without applying outward pressure to the vessel walls.

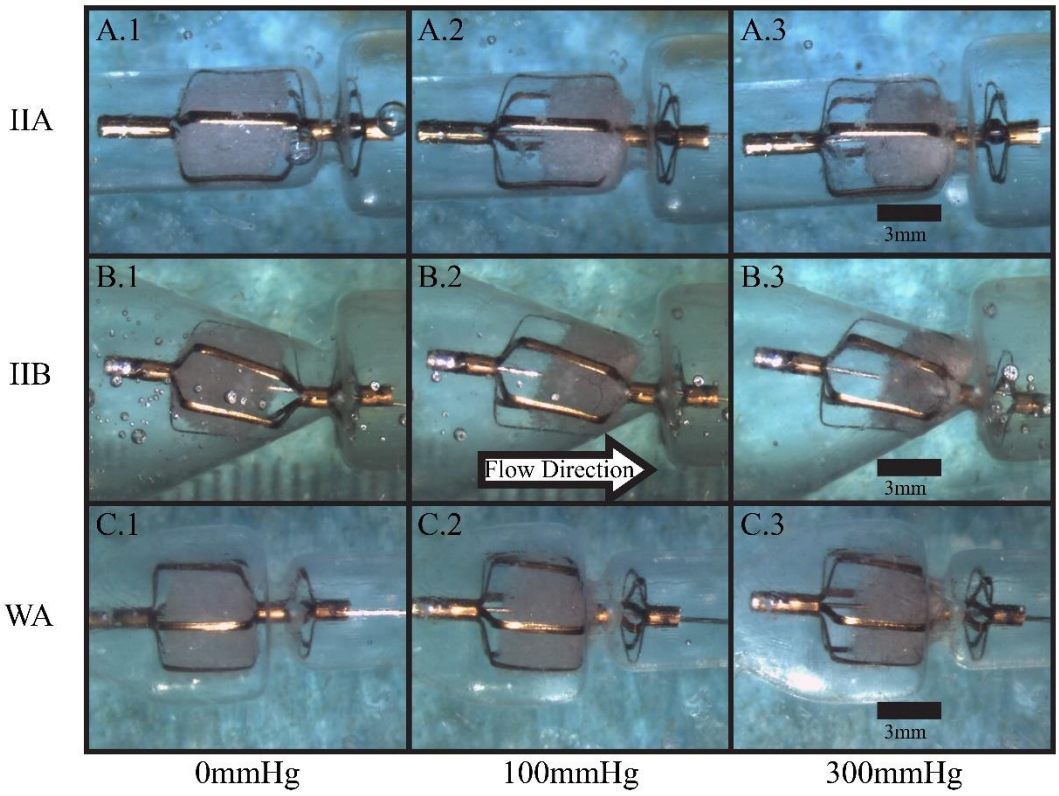

Figure 2.8: Device stability in the IIA (A.1-A.3), IIB (B.1-B.3), and WA (C.1-C.3) models. Flow is from left to right. Images recorded after device subjected to labeled pressures for five minutes.

Table 2.2: Device migration summary. NFC migration at physiological and elevated pressure gradients for each model tested.

Model	NFC Axial Migration (mm)	
Morphology	100mmHg	300mmHg
IIA	0.7 ± 0.3	1.1 ± 0.4
IIB	0.1 ± 0.2	0.8 ± 0.2
WA	0.6 ± 0.4	0.8 ± 0.4

2.3.3.2 Flow Reduction

Flow through the PDA arm was measured with and without a device present at the physiological and elevated pressure gradients. The percent reduction in flow for each pressure and model is shown below in Table 2.3. NFC flow reduction was similar across each model for a given pressure gradient. Flow was impeded to the greatest extent by the NFC in the IIA model at both the physiological and elevated pressure gradients. The ACDO exhibited negligible flow reduction.

Table 2.3: Device flow reduction summary. Percent reduction of flow at the physiological and elevated pressure gradients.

Model Morphology	NFC Flow Reduction		ACDO Flow Reduction
	100mmHg	300mmHg	100mmHg
IIA	60% ± 5%	83% ± 2%	1% ± 0.2%
IIB	51% ± 7%	80% ± 5%	0.6% ± 0.06%
WA	58% ± 5%	78% ± 4%	0.7% ± 0.6%

2.3.4 Physiological Model in vitro Experimentation

2.3.4.1 Device Deployment

The NFC devices were delivered to the geometry without difficulty. Figure 2.9 shows images from the deployment of NFC 1 (Table 2.1). Figure 2.9A shows the NFC being advanced through the catheter to the MPA, Figure 2.9B shows the distal cage deployed, Figure 2.9C shows the distal cage pulled against the pulmonic ostium, and Figure 2.9D shows the entire device deployed. The NFC conformed well to the ductus and remained securely in position, even when the delivery cable compressed the proximal cage during deployment and release. It was noted that the NFC was much easier to advance through the sheath compared to the ACDO.

NFC 3 was easier to deliver than NFCs 1 and 2, due to the larger distal cage. NFC 4 showed improved visualization due to the use of the tungsten doped foam. The clinician could visualize the foam expansion as a reduction in contrast, as shown in Figure 2.10.

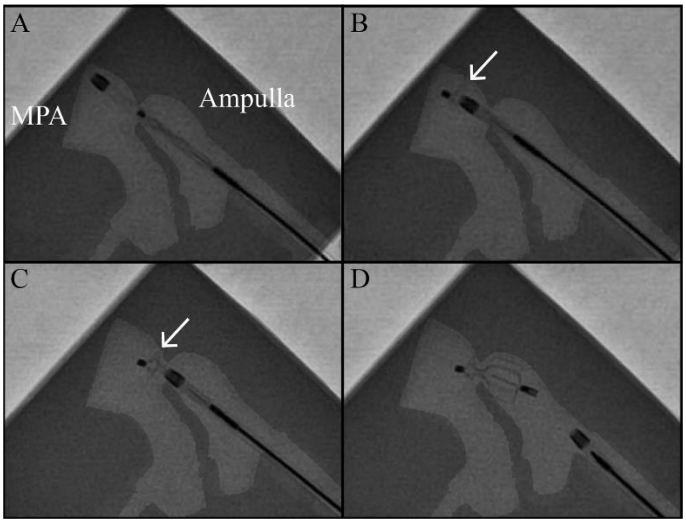

Figure 2.9: NFC deployment (NFC 1) into physiological model under fluoroscopic guidance. A: NFC in catheter. B: Distal cage deployed from catheter. C: NFC placement against pulmonic ostium of model. D: Proximal cage delivered and device released. White arrow indicates distal cage during deployment and positioning.

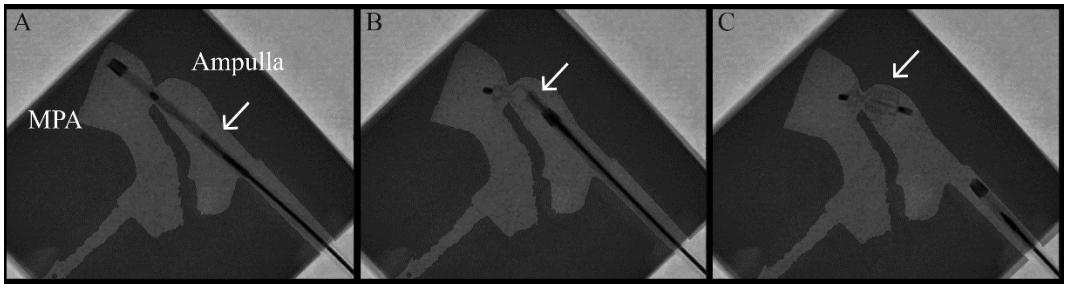

Figure 2.10: Tungsten-doped foam visibility under fluoroscopic guidance during NFC 4 delivery. A: NFC in catheter. B: Proximal cage deployment, foam begins to expand. C: NFC deployed, foam expansion indicated by reduction in the radiographic contrast of foam. White arrow indicates foam location.

2.3.4.2 Device Retraction

NFC retraction into the sheath was assessed using NFC 3 (Table 2.1). The device was deployed as previously described in Section 2.5.2 and after the foam was fully expanded, NFC retraction was attempted while at a physiological pressure gradient of 100mmHg. The clinician successfully retracted the device into the 4Fr sheath by holding the sheath in place and pulling the device cable to recapture the device.

2.3.4.3 Occlusion

The post deployment angiograms of NFCs 1, 2, 4, and the ACDO (Table 2.1) were compared to assess completeness of occlusion. Since no blood was present, the foam could not completely occlude the ductus with thrombus formation, however, flow reduction was expected. Figure 2.11 shows images of the devices within the model during angiograms.

The foam of NFC 1 (Figure 2.11C) did not show appreciable flow reduction as the angiogram appeared similar to the baseline angiogram. It appears that NFCs 2 and 4

provided the best occlusion as indicated by the amount of contrast present in the ampulla during the angiogram (Figure 2.11 D&F). The contrast was slowest to clear in Figure 2.11F, when the pressure gradient was set to 200mmHg. The ACDO showed similar flow reduction to the small foam NFC as indicated by the lighter contrast (Figure 2.11 B&C); NFC's with larger and denser foams show darker contrast on the side of contrast delivery (Figure 2.11 D-F).

2.4. Discussion

2.4.1 Radial Pressure

The ACDO exerted a higher pressure than the NFC at all ampulla diameters tested except at 4mm. The ACDO exerted a higher pressure than the NFC because the OD of the ACDO was 11mm whereas the OD of the NFC was 6.3mm (Figure 2.6). Additionally, the ACDO pressure may be underestimated as the proximal cup shape and waist could not be fully deployed into our test system as it would be deployed *in vivo*.

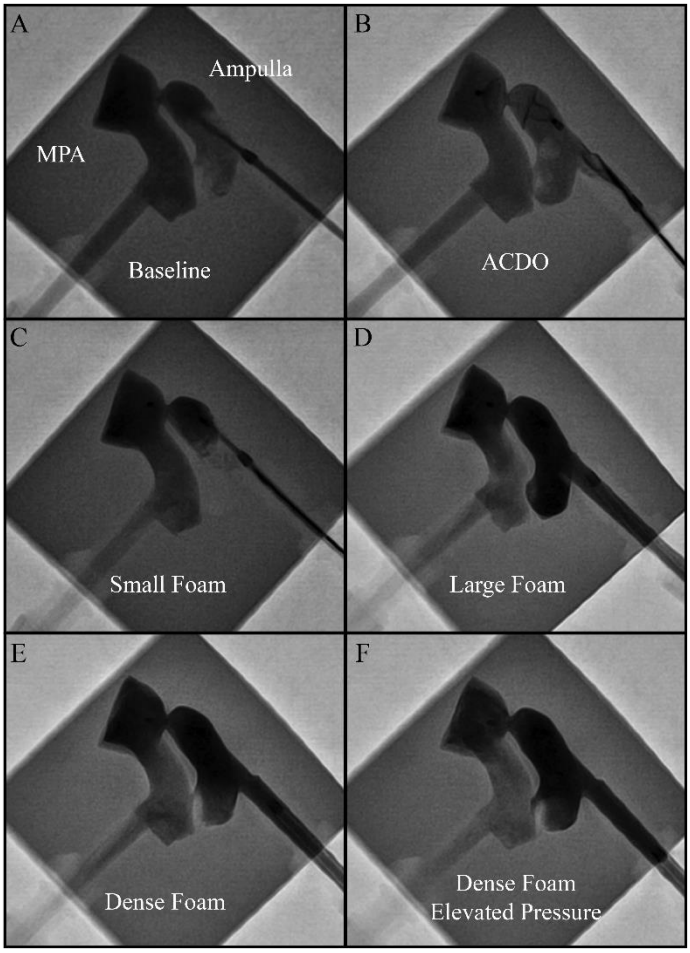

Figure 2.11: Flow reduction comparison. Images were collected at the time when max contrast was present in ampulla as determined by visual inspection. A: Model without a device present to provide a baseline image. B: Model with the ACDO positioned. C & D: NFC devices with a 6 mm diameter and 8 mm diameter SMP foam respectively. E & F: NFC 4 subject to a 100 mmHg and 200 mmHg pressure gradient respectively.

The devices were tested at a range of vessel sizes to determine how the pressure exerted on the wall changed as a function of vessel diameter to ensure that the pressure exerted by an oversized device placed into a small PDA would not burst the vessel. The NFC is designed to be deployed in a PDA with a 5.5 – 6mm ampulla, and an MDD of

3mm. At these diameters, the device exerts approximately 2-11kPa (15-80mmHg) of pressure, which is much lower than the pressure exerted by the ACDO (16-17kPa, 120-128mmHg) and the calculated burst pressure of 200kPa (1500mmHg).

As indicated by the wide ampulla migration studies, radial pressure may not directly correlate to device stability. The oversized device waist and ability for the device to catch on a ductal taper are more important factors when predicting stability. The ACDO has been used to treat tubular PDAs without a ductal taper, but caution is urged when treating this shape because stability only comes from oversizing the device relative to the PDA diameter [1]. The NFC was found to exert pressures much lower than the estimated vessel burst pressure and on the same order of magnitude as the ACDO (Figure 2.6), which indicates that the current NFC design minimizes vessel trauma and the risk of ampulla rupture due to deployment pressure.

2.4.2 Removal Force

The removal force of the ACDO was approximately six times higher than that of the NFC in all models tested (Figure 2.7). The cupped proximal disk and oversized waist of the ACDO increased the device stability and force required to remove it from position, resulting in no visible migration of the device in the *in vitro* tests. Therefore, it was concluded that higher removal forces correspond to increased device stability and reduced migration.

The removal force of the NFC was underestimated as the experiment only evaluated the removal force of the device frame, even with the presence of foam in the

device. In the *in vitro* experiments, the flow compressed the foam against the struts, keeping them flat against the taper of the ampulla, helping the entire device remain in position. In the removal force experiment, flow was not present and the foam was not compressed against the NFC struts. The removal force was lowest in the IIB model because the angled taper of the rigid model did not allow the devices to fully expand; therefore, the struts were already partially collapsed. The removal force was highest in the WA model because the devices were allowed to fully expand, increasing the amount of force required to collapse the struts into the MDD. These experiments would be more representative of *in vivo* conditions if thin walled PDMS models were used instead of the rigid, thick walled models used.

2.4.3 Simplified Model in vitro Experiments

2.4.3.1 Device Stability

Device migration and rotation is not desirable, but it was promising that the proximal cage and foam were not forced through the ductus. There was only one instance in which the struts on the proximal cage partially compressed into the MDD, but the device was not completely forced into the MPA. However, while it is optimal to minimize device protrusion into the MPA, minimal device protrusion has not been reported to cause clinical complications [32]. The ACDO did not exhibit visible migration once positioned, as has been reported in multiple *in vivo* studies [1, 5].

The NFC migration could be due to the rigid PDMS model and fabrication methods used. A thin walled model would more accurately mimic a compliant blood

vessel and allow the device to fully expand and remain anchored in place. While no migration is desired, these initial results are promising and can be improved with future designs by modifying the cage. Decreasing the distance between the proximal and distal cages would allow the proximal and distal cages to better compress the tissue around the MDD.

2.4.3.2 Simplified Model Flow Reduction Experiments

The NFC reduced flow by approximately 50% at the physiological pressure gradient and approximately 80% at the elevated pressure gradient (Table 2.3). It was not expected that the device would achieve 100% occlusion in the absence of blood. The goal of the test was to ensure that flow was being impeded. It has been reported that when similar SMP foams have been placed within blood vessels, clotting and complete occlusion of the blood vessel occurs in approximately two minutes [49]. The NFC reduced flow to a much greater extent compared to the ACDO, which showed negligible reduction. ACDO flow reduction at 300mmHg could not be assessed as the device did not impede flow enough to allow our system to develop this pressure drop. Despite the negligible reduction of flow in water, the ACDO performs very well when implanted clinically [1, 5, 15]. Therefore, as evidenced by the reduction of flow in water and results from Rodriguez et al, the NFC should rapidly occlude the defect on a similar or faster timescale compared to the ACDO (~5-20min) [5, 15].

2.4.4 Physiological in vitro Experiments

The overall response regarding the NFC from the veterinary cardiologist was very positive. The veterinary cardiologist commented that the deployment of the NFC devices offered easy delivery and effortless advancement through the delivery sheath, and was much easier to advance and exhibited much less resistance than the ACDO. The 6 mm ACDO used in this test is designed to be deployed through a 5 Fr sheath, however, it was delivered through a 4Fr sheath per standard clinical use [33]. It is desirable to deliver the devices through smaller delivery sheaths because it expands the population of patients that can be treated [6, 22]. The delivery time of the NFC was similar to that of the ACDO, meaning that the patient and clinician would not be subjected to a larger radiation dose than the current method due to increased procedure time. All NFC devices were properly deployed. Like the ACDO devices, the NFC was easily recaptured into the delivery sheath when repositioning was attempted. Therefore, the device could be retracted if there was an undesirable placement in the clinic. The ACDO did not appear to occlude flow as well as the NFC as indicated by the lighter contrast (Figure 2.11B). However, none of the devices exhibited complete occlusion because the blood clotting capabilities were not present.

2.5 Conclusions

The ACDO is an effective device for canine PDA occlusion, however, its large delivery system and expense limits its use in the clinic. An option that is deliverable in an equal or lower profile system with similar mechanical and occlusion properties and lesser cost is desirable.

The NFC conformed to the proposed requirements, and performed similarly to the ACDO in our tests. One area in which it shows improvement is its scalable aspect. The NFC cage diameter can be adjusted by increasing the length of the laser cut slots, thereby altering its expanded diameter, making it capable of treating large and small PDAs through a 4Fr sheath. The compressed OD is limited to the OD of the nitinol tube or compressed SMP, whichever is larger. Some ACDOs are deliverable in sheaths this size, but not those used to treat larger geometries. Additionally, using a smaller OD nitinol tube may allow for the treatment of canine PDA through even smaller delivery systems such as 4Fr catheters (OD ~1.3mm), further expanding the population of patients that could be treated with the NFC.

The NFC was designed to minimize materials used with the goal of reducing the cost compared to the ACDO. The NFC frame is formed from 1.25” of 0.044” OD, 0.041” ID nitinol tubing, and the ACDO’s frame is composed of two or three 144, 0.0015” – 0.003” nitinol wires [33]. The cost of the SMP foam is negligible. The NFC minimizes materials needed for stability and occlusion (monolithic nitinol frame and SMP foam), compared to the hundreds of wires required for the ACDO. However, while we have shown a reduction of materials used in fabrication, there are other factors that contribute

to device cost, such as manufacturing processes and preclinical testing costs that will be analyzed in future studies.

The current NFC design is dependent upon the ability for the device to fully expand rather than to apply pressure to the vessel wall, as it appeared most stable in the WA model. This is encouraging because even if there is ampulla enlargement post deployment, it should not compromise the treatment as can occur with other endovascular treatment methods [2], further reducing the risk of complications during treatment.

The presented results and the promising clinician feedback obtained indicate that with design refinement, the NFC device could be used to treat canine PDA.

CHAPTER III

SHAPE MEMORY POLYMER FOAM CLOT MIMIC UTILIZING ACRYLAMIDE HYDROGELS

3.1 Introduction

Patent ductus arteriosus (PDA) is a congenital abnormality in which the ductus arteriosus, connecting the aorta to pulmonary artery, does not close shortly after birth. This defect results in continuous left to right shunting of blood, which can lead to serious complications when left uncorrected, such as ventricular dilation, cardiac arrhythmias, congestive heart failure, and even death [1, 2]. PDA is the most common congenital cardiac defect found in canines, occurring in 0.68% of live births, and accounting for 28% of all congenital cardiac abnormalities in dogs [4]. Canine PDA has historically been treated via surgical ligation, a highly invasive treatment in which the chest cavity is opened and the ductus arteriosus is tied off with sutures and excised. More recently, minimally invasive techniques have been developed in an attempt to reduce the operative risk and ease use [1, 33], with the most common device used being the Amplatz® Canine Ductal Occluder (ACDO). While the ACDO is effective at treating PDA, its high cost and large delivery profile limit its use, prompting development of an alternative device [56].

Shape memory polymers (SMP) hold promise in the field of minimally invasive embolic devices. Due to their thrombogenicity and favorable healing properties with minimal inflammation [38, 57], ultra-low density polyurethane SMP foams have been investigated for use in many different applications, including aneurysm occlusion [57, 58],

peripheral embolization [59], and PDA occlusion [56]. Functionally, SMPs are a unique class of materials that undergo shape change upon the application of an external stimulus [34]. In the case of the SMP foams discussed here, the materials are amorphous thermosets that are thermally stimulated around the glass transition temperature (T_g); the SMPs are synthesized in an original expanded foam shape, heated to above their T_g, mechanically deformed to a compressed shape, and cooled to lock in the compressed geometry. This secondary geometry is held until the temperature is raised above T_g and the foam recovers its original, expanded shape. [34, 35]. Water plasticization can be utilized to enable further control over SMP foam-based device storage and actuation. Namely, once the hydrogen bonds in the polyurethane network are interrupted by water molecules, the T_g is effectively lowered. Thus, SMP foams are designed to remain stable under dry conditions and actuate upon exposure to the water in blood at body temperature, upon which they expand and absorb blood. The foam induces thrombosis through the intrinsic clotting cascade, and thrombus forms throughout the foam matrix [59].

Typically, foam prototypes are evaluated without the use of blood or thrombi [56, 58, 59]. However, it is important to evaluate device mechanical properties and performance after clotting. To this end, polyacrylamide hydrogels were chosen as a clot mimic due to the ability to tailor their mechanical properties by simply varying the concentrations of the acrylamide and bis-acrylamide monomers [60]. Additionally, polyacrylamide hydrogel clot mimics were previously used to investigate clot capture performance of inferior vena cava filters [61-63]. In the current work, SMP foams were doped with varied compositions of polyacrylamide hydrogels in effort to match the

modulus of a blood-clotted foam in two different pore size ranges. The clot mimic foam was then incorporated into a prototype PDA device to gain an understanding of device properties after implantation and clotting has occurred. Here, we focused on characterizing PDA prototype dislocation force before and after clotting.

Devices indicated to treat PDAs must withstand many forces, including a 100 mmHg pressure gradient across the ductus that can increase to 200 mmHg acutely [personal communication, Matthew W Miller]. Prototypes have been tested at these pressures, but a second measure of stability is the force required to push the device through the minimal ductal diameter (MDD) after deployment in the PDA. This dislocation force measures device stability within the PDA and provides a comparative measure of frame stability across different device types. It was hypothesized that dislocation force increases after foam clotting, in turn decreasing the likelihood of device migration, which could occur due to ampulla enlargement or acute pressure increases. Frame stability during device placement is another important design consideration. When implanting these devices, clinicians push and pull the delivery cable after positioning the device to ensure that the device is stable [15]. If the dislocation force is excessively low, the devices get pushed through the PDA anatomy during positioning and cannot be confidently placed in the correct position.

3.2 Materials and Methods

3.2.1 Materials

N,N,N′,N′-tetrakis (2-hydroxypropyl)ethylenediamine (HPED) (99%; Sigma–Aldrich), triethanolamine (TEA) (98%; Sigma–Aldrich), and hexamethylene diisocyanate (HDI, TCI America Inc., Portland, OR) were used to synthesize the SMP foams. Additional foaming components included surfactants, DC 198 and DC 5943 (Air Products and Chemicals, Inc., Allentown, PA), catalysts, T-131 and BL-22 (Air Products and Chemicals, Inc., Allentown, PA), and a physical blowing agent, Enovate 245fa (Honeywell International Inc, Morristown, NJ). Hydrogels were synthesized using 40% (w/v) acrylamide stock solution (Sigma-Aldrich), 2% (w/v) bis-acrylamide stock solution (Sigma-Aldrich), tetramethylethylenediamine (TEMED) (Sigma-Aldrich), and ammonium persulfate (APS) (Sigma-Aldrich). The hydrogel stock solutions were stored at 4°C when not in use.

3.2.2 Foam Preparation

Foams were prepared following the three-part process described in Hasan et al [52]. Briefly, appropriate molar ratios of HDI, TEA, and HPED were reacted over two days to form an isocyanate (NCO) prepolymer. Then, a hydroxyl (*OH*) monomer mixture was prepared by mixing molar ratios of TEA, HPED, a small amount of deionized water, and catalysts. The NCO and *OH* mixtures were combined with surfactants and blowing agents, mixed, and poured into a foam bucket to react and cure. By tailoring the viscosity of the premixes, large (1970 ± 240 um transverse pore diameter) and small (650 ± 130 um

transverse pore diameter) pore foams were fabricated. Figure 3.1 shows images of the transverse and axial pores, and Table 3.1 displays the full pore size characterization of the foams used. Foam was sectioned into 7 x 6 x 3 cm blocks and reticulated following the method described previously [49]. The blocks were then conditioned by compressing and expanding them at 100°C. Cylinders with a diameter of one centimeter were punched out of the reticulated, conditioned block, cleaned through multiple sonication and tumble cycles in isopropyl alcohol and water, and freeze-dried to preserve their cylindrical geometry. Foam cylinders with diameters between 9.5 – 10 mm and heights between 6.6 – 6.9 mm were cut from the freeze-dried cylinders for testing.

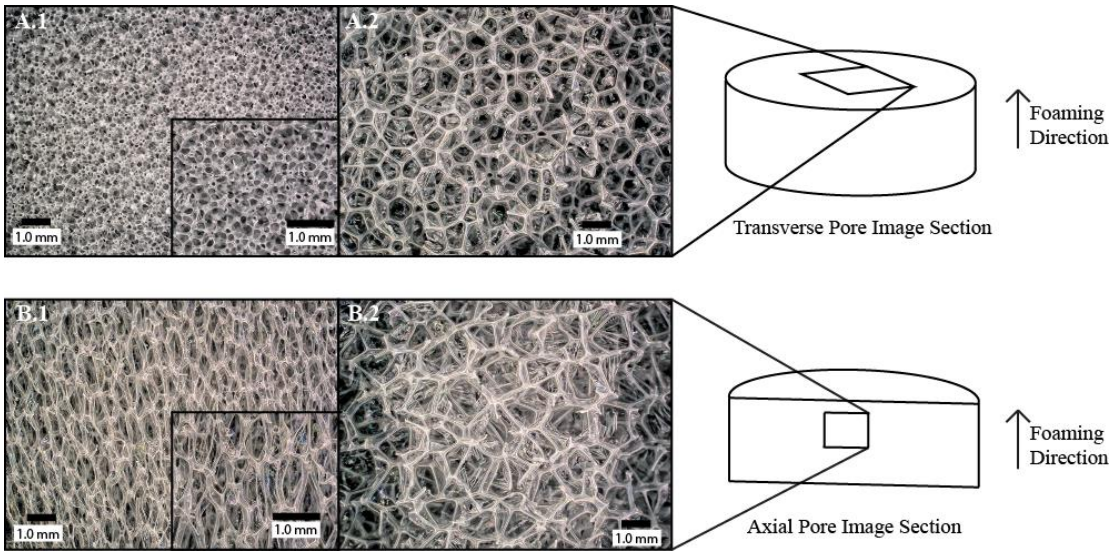

Figure 3.1: (A) Transverse and (B) axial pore images of (1) small and (2) large pore foams.

Table 3.1: Pore size characterization of small and large pore foams. Aspect ratio defined as the length of the pore in the foaming direction/length of pore in the radial direction.

	Transverse Pore Diameter	Axial Pore Diameter		Axial Pore Aspect Ratio
		Long Axis (Foaming Direction)	Short Axis (Radial)	
Small Pore Foam	**650 ± 130 um**	**1310 ± 240 um**	**530 ± 100 um**	**2.5 ± 0.5**
Large Pore Foam	**1970 ± 240 um**	**1980 ± 400 um**	**1620 ± 190 um**	**1.2 ± 0.3**

For each pore size, three variants were tested in this study: bare, blood-clotted, and hydrogel-clotted foams (Figure 3.2). Bare foam refers to the clean SMP foam with no fillers. Small and large pore bare foams are denoted SPB and LPB, respectively.

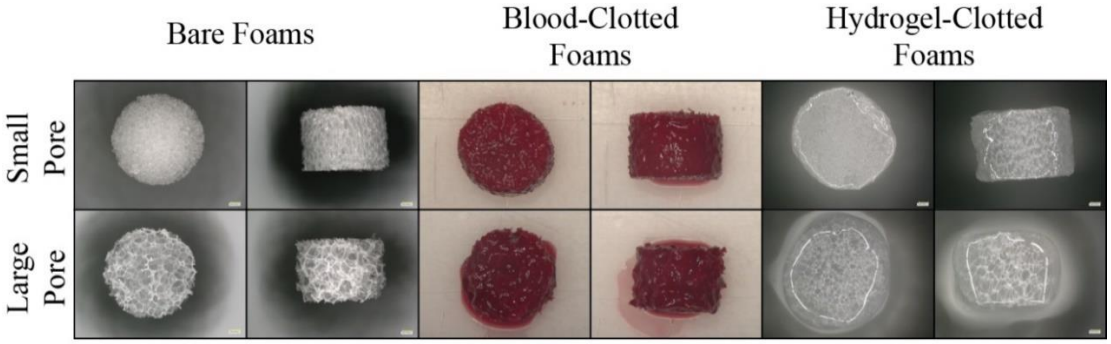

Figure 3.2: Top and side view of small and large pore bare, blood-clotted, and hydrogel-clotted foams. Foams displayed are 10 mm in diameter.

3.2.3 Blood-Clotted Foam Preparation

Bovine blood was acquired from the Rosenthal Meat Science and Technology Center (Texas A&M University in College Station, TX) as a part of a tissue share program. The blood used in this study was collected from animals euthanized for purposes unrelated to this research. The blood was citrated in a 3.2% sodium citrate solution prepared in phosphate buffered saline (PBS). The citrated blood was stored at 4°C until use. Foam cylinders were plasticized in warm PBS, compressed to remove most of the saline, and placed in an acrylic well plate (1 cm diameter wells). Then, the citrate was counteracted using 10 mM calcium chloride [59]. Blood was deposited into each well, which caused the foams to expand. The foams were gently manipulated with tweezers while inside the well to minimize air bubbles and then allowed to fully expand. Following expansion, the plates were covered and incubated at 37°C for 2 hrs to clot the blood within and around the foams [61]. The blood-clotted foams were stored at 4°C and warmed up to room temperature for 24-48 hours prior to modulus measurements using dynamic mechanical analysis (DMA). Small and large pore blood-clotted foams are denoted SPC and LPC, respectively.

3.2.4 Hydrogel-Clotted Foam Preparation

Polyacrylamide clot mimics were fabricated following a protocol by Tse et al. [60]. Briefly, both acrylamide components were combined with water at the volumes designated in Table 3.2. All gels were fabricated with 3% acrylamide, and the bis-acrylamide (bis) concentration was varied to achieve the desired modulus. Then, 10% APS was added at a

1 vol% concentration, and TEMED was added at 0.1 vol%. The solution was vortexed and immediately deposited onto foams in 1 cm diameter well plates, as described above in *Blood-Clotted Foam Preparation*. Following foam expansion, the wells were covered and held at room temperature for 30 minutes to allow the hydrogel to crosslink. The hydrogel-clotted foams were then removed from the wells and stored overnight in reverse osmosis water. Small and large pore hydrogel-clotted foams are denoted SPH and LPH, respectively. The hydrogel compositions used were selected based upon preliminary data which suggested that these monomer compositions would result in hydrogel-clotted foams with moduli that were approximately equal to the blood-clotted foam moduli.

Table 3.2: Hydrogel compositions used for hydrogel-clotted foam preparation.

	Gel Composition		40% Acrylamide Solution (mL)	2% Bis-Acrylamide Solution (mL)	10% APS solution (mL)	TEMED (mL)	Water (mL)
	Acrylamide	Bis-Acrylamide					
Small Pore Foam	3%	0.085%	0.75	0.425	0.1	0.01	8.825
	3%	0.080%	0.75	0.400	0.1	0.01	8.85
	3%	0.075%	0.75	0.375	0.1	0.01	8.875
Large Pore Foam	3%	0.045%	0.75	0.225	0.1	0.01	9.025
	3%	0.035%	0.75	0.175	0.1	0.01	9.075
	3%	0.0325%	0.75	0.1625	0.1	0.01	9.0875

3.2.5 Dynamic Mechanical Analysis of Foam Samples

Foams were tested using immersion clamps on a q800 DMA (TA Instruments, New Castle, DE). Samples were loaded into the compression clamps, and 37°C PBS was added to the base of the top compression plate. The storage and loss modulus were measured by performing a kinetic experiment [58, 64, 65] with the samples subjected to

1% strain at a frequency of 1 Hz. The oven temperature was ramped to 37°C, and the test was carried out for at least 45 minutes until the storage modulus plateaued. Six samples of each foam formulation were tested.

3.2.6 Nitinol Foam Cage Prototype Fabrication and Preparation

PDA prototypes, termed the nitinol foam cage (NFC), were fabricated similar to those described in Wierzbicki et al. [56]. Briefly, ten equally spaced radial slots were excimer laser cut (Resonetics, Nashua, NH) into straight nitinol tubing (NDC, Fremont, CA). Following deburring, the laser-cut tubes were secured in custom fixtures and compressed to conform to the desired frame geometry. The nitinol was shape-set at 550°C for 25 minutes followed by a water quench. The proximal and distal ends of the nitinol frame were then cut to length, and a threaded, stainless steel hypotube was affixed to the proximal end to allow for detachment of the device from the delivery rod. The monolithic frame consists of multiple distinct cages. The flat disc-like distal cage rests against the pulmonary artery wall and serves as a landmark during deployment for the clinician. The proximal cage serves as the anchor point for the SMP foam and applies an outward force to the ampulla to aid in device stability. The waist is a narrow portion between the proximal and distal cages that resides within the MDD. The waist is designed to be two times the diameter of the MDD and serves as the main stability mechanism for the NFC.

3.2.7 PDA Model Fabrication

The dislocation force of NFC prototypes and a commercial Amplatz® Canine Ductal Occluder (ACDO) were evaluated in simplified models of the most common types

of canine PDAs (Figure 3.3), including the cylindrical IIA, the conical IIB, and wide ampulla for cases in which the ampulla expands post occlusion [2, 7, 8]. Construction of the thin walled silicone models is detailed in previous work. The waist of the NFC and ACDO devices is designed to be two times oversized relative to the MDD of the PDA. To assess the influence of proper device sizing on the dislocation force, devices were deployed into two different diameter MDD models, 3 and 5 mm (2x and 1.2x oversized relative to the MDD).

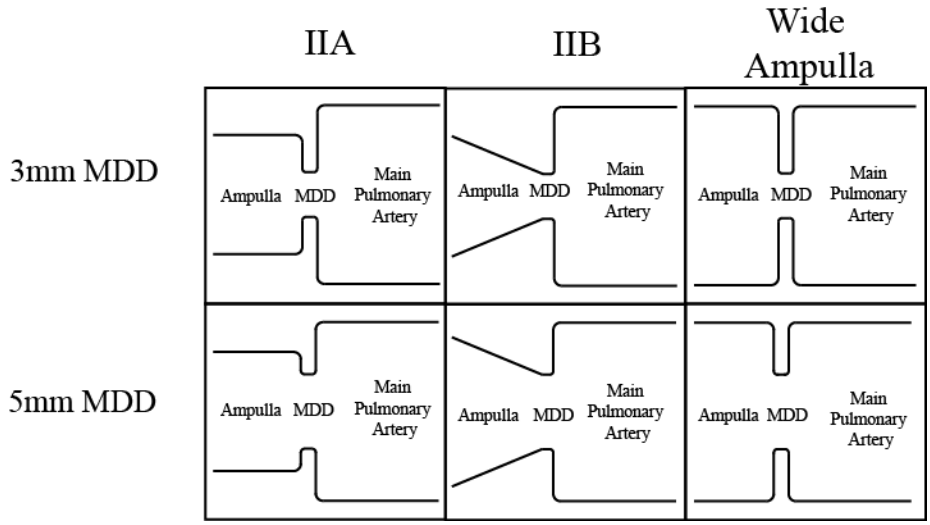

Figure 3.3: Simplified schematics of PDA models used in dislocation force testing.

3.2.8 Dislocation Force Testing

The dislocation force of a 6 mm waist ACDO was compared to that of 6 mm waist prototypes with bare and hydrogel-clotted small and large pore foams. The foams (8 mm diameter cylinders) were prepared as described in *Foam Preparation*. Hydrogel-clotted

foams were frozen at -20°C and freeze dried following polymerization. Once lyophilized, both bare and hydrogel-clotted foams were compressed in a heated stent crimper to a minimal diameter. Compressed foams were glued to the interior proximal end of the nitinol frame, and trimmed to the length of the cage. Figure 3.4A-E show the ACDO and NFC devices with compressed and expanded bare and hydrogel-clotted foams. Each device was loaded into a thin walled silicone model of a PDA geometry, with the distal cage placed within the modeled pulmonary artery, the waist placed within the MDD, and the proximal cage placed within the ampulla (schematic shown in Figure 3.4F) and placed in 50°C water for an appropriate amount of time to fully actuate the SMP foam. A threaded rod was attached to the proximal end of the NFC, and the model with the prototype was placed into a water bath (35-37°C) positioned on an Instron 5965 test frame (Instron, Norwood, MA) (Figure 3.4G). The rod, extending from the proximal end of the NFC, was secured to the Instron grip. The crosshead was lowered at a rate of 2 mm/min until the device was completely pushed through the minimal ductal diameter into the modeled pulmonary artery. The force was recorded throughout the test using Instron Bluehill® 3 testing software, and the dislocation force was recorded as the maximal force recorded during the test. For each permutation, three devices were tested one to three times each.

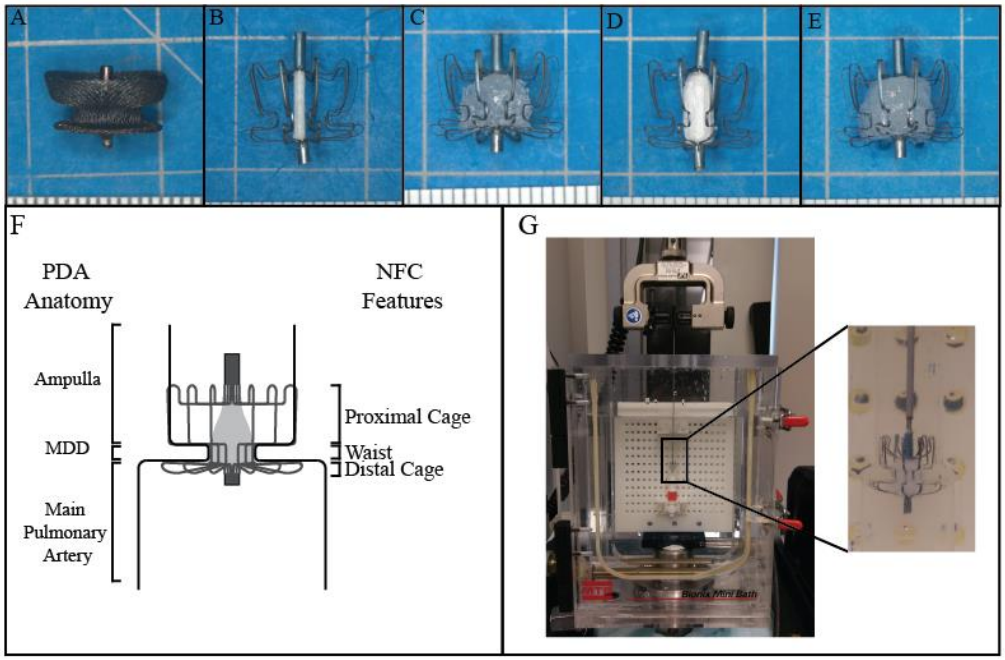

Figure 3.4: Dislocation force testing summary. A: ACDO. B: NFC with compressed bare foam. C: NFC with expanded bare foam. D: NFC with compressed hydrogel-clotted foam. E: NFC with expanded hydrogel-clotted foam. F: Schematic of proper NFC deployment in idealized IIA PDA geometry. G: Dislocation force setup with NFC loaded onto Instron prior to test start. A-E: Scale in mm.

3.2.9 Statistical Analysis

Two-sided analysis of variance (ANOVA) with Tukey multiple comparison analysis, comparing the mean of each sample with the mean of every other sample, was used to compare differences in storage moduli of small and large pore, bare, blood-clotted, and hydrogel-clotted foams. Dislocation force comparisons were analyzed using a two-sided ANOVA with Tukey multiple comparison analysis. Two analyses were performed to assess multiple comparisons, one comparing dislocation force differences across foam types, and a second comparing dislocation forces across PDA models. In instances in which multiple measurements were recorded for the same prototype frame, the average

was first computed for the replicates and the final average and standard deviation was calculated from the averaged replicate measurements of each prototype. In all cases, significance was determined with a level of 95% ($p<0.05$). All statistics were performed using Graphpad Prism 7 (Graphpad Software, Inc, La Jolla, CA).

3.3 Results and Discussion

3.3.1 Dynamic Mechanical Analysis

A series of bare, blood-clotted, and hydrogel-clotted foams were characterized at 37°C to find a hydrogel clot mimic composition with comparable modulus to that of blood-clotted foams. The resulting storage, loss, and complex moduli are shown in Table 3.3, and a comparison of storage moduli are displayed in Figure 3.5. The storage moduli of the bare small and large pore foams were not statistically different. Blood-clotted foams had increased storage moduli relative to bare foams, with a larger increase observed in the small pore blood-clotted foams. Statistical comparison of SPC and SPH formulations revealed that there were no significant differences ($p<0.05$) between the moduli of the SPC and that of any SPH formulation; however, modulus decreased with decreasing bis-acrylamide concentration, following trends reported by Tse et al. [60]. A significant difference was observed between the 0.085% and 0.075% bis-acrylamide composition SPH foams. The increase in modulus between the LPB and LPC foams was not significant. Like the small pore foams, there were no significant differences between any of the LPC and LPH compositions, but there was the similar trend of decreasing moduli with decreasing bis-acrylamide concentration from 0.045% to 0.035%. The moduli of the

0.035% and 0.0325% compositions were relatively unchanged. As the means of the SPH with 0.08% bis-acrylamide and the LPH with 0.0325% bis-acrylamide most closely matched those of the SPC and LPC, respectively, these formulations were selected as the compositions for further studies (hereby simply designated as SPH and LPH).

Table 3.3: Storage, loss, and complex moduli of all foam compositions.

	Storage Modulus (kPa)	Loss Modulus (kPa)	Complex Modulus (kPa)
Small pore bare	1.3 ± 0.7	0.5 ± 0.2	1.4 ± 0.7
Small pore clot	4.3 ± 0.6	2.0 ± 0.5	4.8 ±0.6
Small pore hydrogel 0.085% bis	5.1 ± 0.8	1.0 ± 0.2	5.2 ±0.8
Small pore hydrogel 0.080% bis	4.5 ± 1.0	1.1 ± 0.3	4.6 ± 1.0
Small pore hydrogel 0.075% bis	3.2 ± 0.8	1.1 ± 0.4	3.4 ±0.9
Large pore bare	0.9 ± 0.5	0.5 ± 0.5	1.1 ± 0.4
Large pore clot	1.7 ± 0.3	0.8 ± 0.4	1.8 ±0.4
Large pore hydrogel 0.045% bis	2.5 ± 0.7	0.3 ±0.1	2.5 ± 0.7
Large pore hydrogel 0.035% bis	1.9 ± 0.4	0.6 ±0.5	2.0 ± 0.4
Large pore hydrogel 0.0325% bis	1.8 ± 0.3	0.4 ± 0.3	1.9 ± 0.3

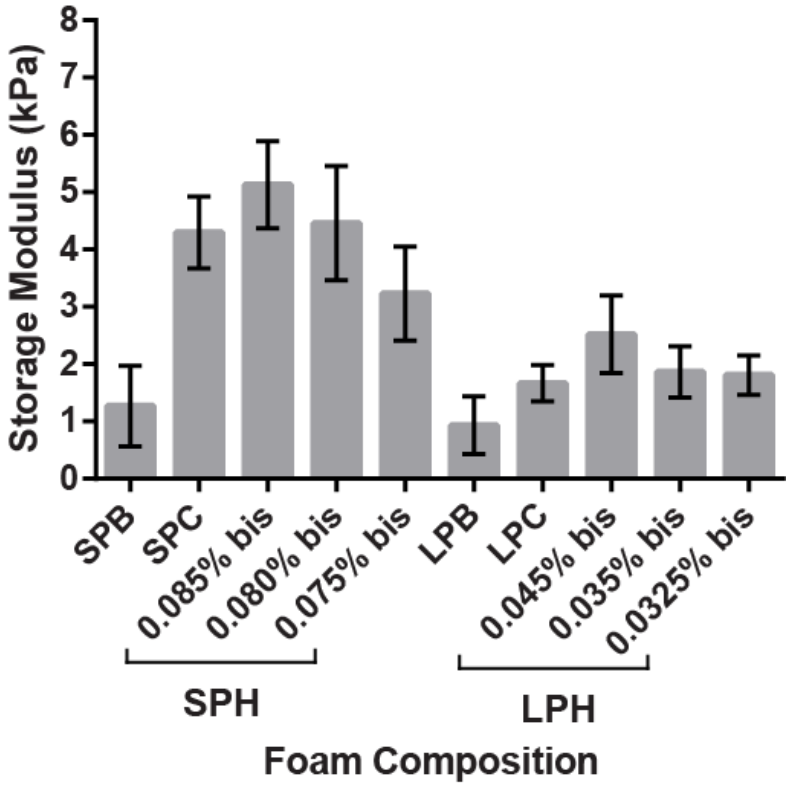

Figure 3.5: Mean storage modulus of prepared foam compositions. SPB: Small pore bare; SPC: Small pore clot; SPH: Small pore hydrogel; LPB: Large pore bare, LPC: Large pore clot; LPH: Large pore hydrogel. All hydrogel-clotted foams made with 3% acrylamide. Bis-acrylamide concentration noted below each respective column.

We hypothesize that the shape of the pores in the foams influenced the modulus of the clotted foams, resulting in a larger increase in modulus after clotting the small pore foams. When a 1600 μm length of LP foam is compressed, there are two struts to resist compression (short axis axial pore size is 1620 μm). When clotted, there is material in the pore, but the struts are still able to bow out and are thus less resistant to compression. For the same length of foam in the small pore foams, there are three struts with clot filling the cells in between (short axis axial pore size is 530 μm). Thus, the outer struts would bow

out under compression, but the middle strut would be supported by the clot and be more resistant to buckling. The higher number of vertical struts in the small pore foam compared to that in the large pore provides a greater resistance to applied compression. The minimal difference in modulus between the SPB and LPB foams was not statistically significant and could be attributed to the lack of a physical constraint within individual pores, allowing for buckling of struts rather than reinforcement. Furthermore, the axial pores of the small pore foams are less isotropic compared to those of the large pore foams, with aspect ratios (length of pore in foaming direction/length of pore in radial direction) of 2.5 ± 0.5 and 1.2 ± 0.3 (Figure 3.1 B.1 and B.2; Table 3.1), respectively. The clots within the relatively columnar pores of the small pore foams better resist compression compared to the more spherical clots formed in the large pore foams. When compressed, the SPC foams have higher stiffness in their taller struts in addition to the constraint of the fibrin mesh in the pores.

3.3.2 Dislocation Force

Upon selection of suitable hydrogel compositions for the clot mimics, the dislocation forces were measured in an immersion chamber held at 35-37°C in each PDA model for all prototype device and foam compositions in comparison to the commercial ACDO, Figure 3.6. Overall, the ACDO exhibited a significantly higher dislocation force than all prototypes. There were minimal differences in the dislocation forces of the prototypes; however, the dislocation forces of prototypes containing small pore foam were

approximately equal to or slightly higher than that of prototypes containing large pore foams for each model, as was expected.

In general, the 3 mm MDD models resulted in higher dislocation forces compared to the 5 mm MDD models, because each device was forced through a smaller orifice. This difference was significant for all foam types and ACDO devices in the IIA and IIB models ($p<0.05$), except for the LPH foams in the IIB models. The large standard deviation in the IIB 3 mm SPH prototypes is partly due to the setup. Namely, the diameter of the SPH was too large for deployment across the 3 mm MDD as shown in Figure 3.4F,G; therefore, the foam was deployed entirely in the ampulla. For all other prototypes, the foam was deployed across the MDD. In some runs with the SPH in the IIB 3 mm model, the cage was not forced through the MDD axially, and the pushing rod rubbed the side of the model, increasing variability and resulting in a higher standard deviation. The wide ampulla models resulted in similar dislocation forces for both the 3 and 5 mm MDD, with the largest decrease seen in the SPH samples, indicating that stability could be influenced by the ratio between the ampulla and minimal ductal diameter.

It was expected that the dislocation force would increase between the bare and hydrogel-clotted foams; however, they were very similar in these tests, and there was not a significant difference between SPB and SPH or LPB and LPH prototypes for a given model. The minimal difference between bare and clotted foams is important, because it shows that the ability to resist dislocation is not negatively or positively impacted by clotting. However, we hypothesize that fibrin in the thrombus and mature connective tissue would better bind the foam to the vessel wall over time [38, 57], which could

increase the dislocation force *in vivo*. It should be noted that lyophilization, compression, and rehydration of the foam may alter the modulus from values presented in *Dynamic Mechanical Analysis* results.

While the differences in dislocation forces are small, these experiments still provide important design considerations for embolic devices. Dislocation force is primarily dictated by the nitinol cage rather than other variables, such as foam pore size or clot presence. Although the dislocation force of the prototype is approximately three times lower than the ACDO, this result does not indicate that the prototypes will not withstand the necessary physiological pressures. Other *in vitro* stability tests analyzing migration have shown stability under relevant pressures [56]Wierzbicki 2017 in prep]. Dislocation force is also an important characteristic in user deployment. Following placement of PDA devices, clinicians apply a gentle 'to and fro' motion to ensure that the device is securely positioned [15]. During previous *in vitro* studies, a clinician noted that it was much easier to push the prototype through the MDD compared to the ACDO, indicating that increasing the dislocation force of the prototypes could be beneficial. Thus, future work will focus on increasing the dislocation force of the device while still maintaining the desirable properties relative to the ACDO.

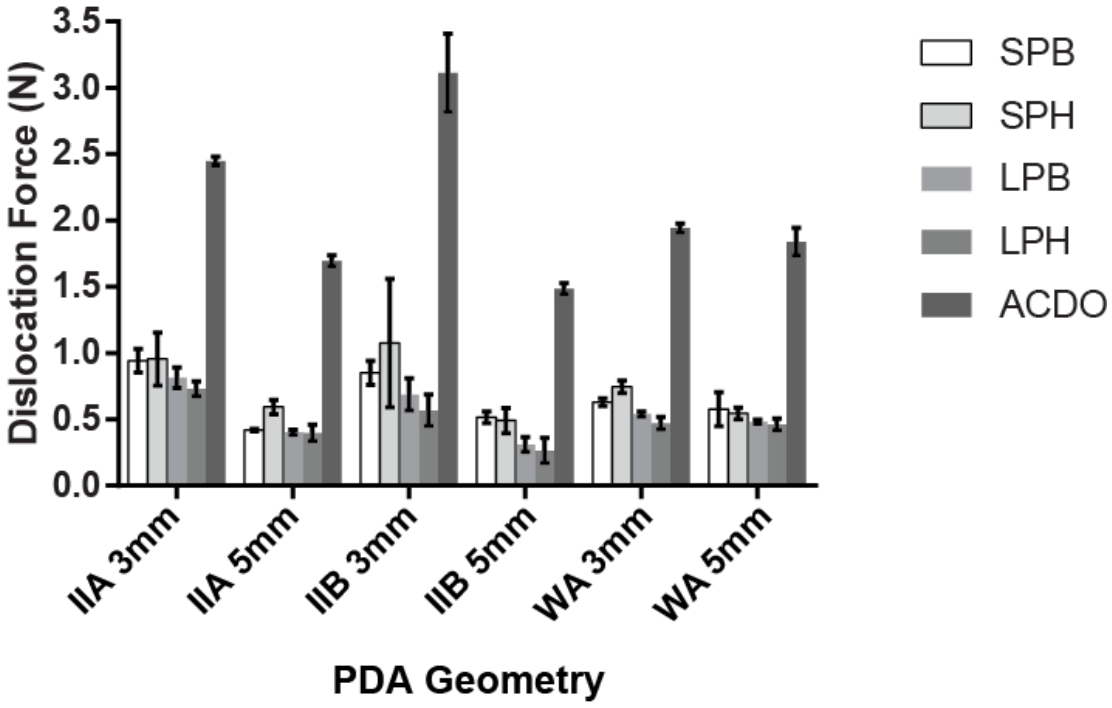

Figure 3.6: Dislocation force of for each prototype/foam combination and the ACDO in each PDA model.

3.4 Conclusions

This study showed that the dislocation force is not significantly affected by the increased modulus of the foam after clotting. The rigidity of the nitinol frame is most influential on dislocation force and masks the effects of clotting within the foams. Foam pore size has a small effect on dislocation force. This result is partially because the foams are expanded across the MDD in ideal deployments. Thus, the foam does not have to be compressed through the MDD during dislocation.

In addition to the dislocation force tests described here, these composite materials are useful for studying the stability and flow reduction of devices following occlusion. Wierzbicki et al. and Landsman et al. evaluated stability of two different prototype SMP

foam-based devices at physiological and elevated pressure and flows using bare foam devices. The bare foam increases resistance to flow, but does not completely occlude the vessel, which would occur physiologically once thrombus formed throughout the device [59]. Using a clotted foam device in a setup similar to that described previously [66, 67], which analyzes how the device restores normal flows and pressures following occlusion of the shunt, could be beneficial during prototype development to better predict *in vivo* behavior under controlled conditions.

An additional advantage to using hydrogel-clotted materials is ease of handling. Acquiring, storing, and using whole blood greatly increases the difficulty and decreases the efficiency in which studies can be performed due to the added complications and preparation required. Hydrogel-clotted foams can be readily prepared with off-the-shelf hydrogel materials and integrated into study design without the added complications of biohazardous materials and blood handling to more rapidly screen device compositions.

A limitation to using these materials in *in vitro* tests is that the lyophilized hydrogel foam cannot be compressed to as small of a diameter as the bare foams that would be used in the actual application. Thus, the devices may have to be deployed through larger catheters for the experiment or manually positioned using a different method. While a limitation, hydrogel-clotted foam devices can still provide valuable information if they can be positioned correctly. Also, as the primary use of these materials is the evaluation of device performance post occlusion, deployment characteristics can be assessed on bare foams through separate benchtop studies. Overall, these studies provide (1) a platform

technique for consistent evaluation of the effects of clotting and (2) more information on a potentially valuable technology to treat PDAs.

CHAPTER IV

AN EXPERIMENTAL CANINE PATENT DUCTUS ARTERIOSUS OCCLUDER BASED ON SHAPE MEMORY POLYMER FOAM IN A NITINOL CAGE

4.1 Introduction

Patent ductus arteriosus (PDA) occurs when a normal fetal connection between the aorta and pulmonary artery does not close shortly after birth, leading to a continuous left-to-right side shunting of blood. When left uncorrected, the PDA leads to many complications including congestive heart failure and death [1, 2].

PDA is the most common congenital cardiovascular defect that occurs in canines, manifesting in 6.8 out of 1000 live births and comprising approximately 28% of all congenital cardiovascular defects [4]. PDA has been traditionally treated via surgical ligation, in which the chest cavity of the dog is opened via thoracotomy and the ductus is ligated [1, 3, 47, 48]. While effective, surgical ligation is highly invasive, and carries non-trivial operative risks including, nonfatal hemorrhage, pneumothorax, and chylothorax as reported in 11-15% of cases [16-19] and operative mortality in up to 11% of cases [3, 16-19, 47], which increases the attractiveness for a minimally invasive closure techniques [6].

Many endovascular devices intended for human PDA and peripheral occlusion, such as embolization coils, the Amplatzer™ Duct Occluder (ADO), and the Amplatzer™ Vascular Plug (AVP), have been investigated as options to treat the canine PDA. While there has been some success using current human devices within the canine anatomy, complications such as completeness of occlusion, device migration, delivery system size,

and ease of delivery has limited their use [2, 5, 6, 9, 21, 22, 24, 25, 27] and led to the development of the Amplatz® Canine Ductal Occluder (ACDO) [1, 33]. The ACDO is very successful in PDA closure treatments, yet is still limited by cost and its relatively large delivery system profile. While some advances have been made to reduce the profile [68], the smallest sheath that current commercial devices can be delivered through is still a 4Fr sheath, restricting the size (body weight) range of dogs that can be occluded percutaneously.

A prototype nitinol foam cage (NFC) device that utilizes shape memory polymer (SMP) foams has been developed as previously described in Wierzbicki et al [56] with design modifications to the shape for improved stability and increased foam capacity. The NFC prototype utilizes an SMP polyurethane foam, rather than a dense nitinol mesh to occlude flow. SMPs are a unique class of materials that can be heated above a characteristic glass transition temperature (T_g) and when deformed and cooled below the T_g, hold a secondary shape. The polymer can then be actuated back to its original configuration through an entropy driven process by increasing the temperature of the polymer above its T_g via an external stimulus such as heat or contact with body temperature blood [35]. The unique mechanical and embolic properties of these materials have led to the investigation of multiple biomedical embolic device applications for endovascular occlusion [39, 40]. Multiple *in vitro* and *in vivo* studies have been conducted demonstrating the favorable occlusion and biocompatible properties of these materials, as shown through occlusion within 2 minutes once implanted [49] and minimal inflammation

characterized by dense tissue growth and collagen deposition at 90 days post-implant, prompting investigation for their use in other embolization applications [38].

The prototype NFC discussed herein is constructed from one continuous nitinol conduit with three sections: the proximal cage, waist, and distal cage, and inclusion of SMP foam. In endovascular deliveries, the distal cage is advanced out of the catheter first and pulled against the pulmonary artery wall, serving as an anchor point and landmark for the device and clinician, respectively. The waist is designed to be oversized relative to the minimal ductal diameter (MDD) by approximately 2x, such that it will apply an outward force to the ductus, aiding in stability. The proximal cage expands to apply pressure to the ampulla wall and is the attachment region for the foam. The SMP foam is anchored within the proximal cage and spans and fills all three sections of the frame.

Through discussions with clinicians, multiple design criteria were defined to determine device success. First, the device must be deliverable through a 4 Fr sheath having an internal diameter of 1.3 mm or smaller as larger sheaths and catheters cut out a large subset of the canine population that can be treated with minimally invasive devices. Additionally, the prototype must be retractable into the sheath in the event of an improper deployment or sizing, be visible under fluoroscopy following delivery, and remain stable once deployed at physiological and elevated pressures. Fabricated NFC prototypes were tested against ACDO performance in multiple verification tests to evaluate strut integrity and nitinol frame radial forces, as well as stability and deployment characteristics in simplified and physiological PDA models, respectively, under experimental flow conditions.

4.2 Methods

4.2.1 Device Fabrication

NFC prototypes were fabricated in a similar way to those described in Wierzbicki et al [56]; however, two variations in wall-thickness were used to assess differences regarding the effects of strut stiffness on the prototype's deployment characteristics. Briefly, the NFC prototypes were fabricated by cutting ten equally spaced slots radially into a straight nickel titanium alloy (nitinol) tubing using an excimer laser (Resonetics, Nashua, NH). The thin-walled prototypes (NFC_{Tn}) were constructed using 0.044" outer diameter (OD) and 0.041" inner diameter (ID) (NDC, Fremont, CA) tubing (0.0015" wall thickness), while the thick-walled prototypes (NFC_{Tk}) were constructed using 0.044" OD and 0.040" ID (Vascotube, Birkenfeld, Germany) tubing (0.002" wall thickness).0.002" wall thickness. One continuous slot was used to form the cage in this design, rather than two consecutive slots used previously. The laser cut nitinol tubes were deburred using abrasive paper and sonicated in isopropyl alcohol. Custom fixturing compressed the tubing, while allowing the struts to expand to the desired shape with a waist of 6 mm OD, shown in Figure 4.1. The final shape was defined by annealing the nitinol frame and fixture within a furnace held at 550℃ for twenty-five minutes, followed by a water quench. A threaded release mechanism was laser welded to the proximal end of the device and an 8 mm OD, 5 mm length SMP foam was compressed to a minimal diameter and epoxied into the lumen of the proximal portion of the device. Figure 4.2 illustrates a comparison between the ACDO and the NFC_{Tn} prototype with a compressed and expanded foam insert. Additionally, a subset of thick walled prototypes (NFC_{Tk}) were electropolished

(NFC_{TkEP}) (Able Electropolishing, Chicago, Il) to a wall thickness of approximately 0.0015" to evaluate how electropolishing influenced frame durability and fatigue life.

4.2.2 PDA Model Fabrication

While the PDA morphology varies from animal to animal, there are three basic geometries the ductus arteriosus may manifest that vary in size and shape [7]. Simplified thin walled silicone models were fabricated with shapes based on those described by Miller et al [7], including the cylindrical (IIA) and elliptical ampulla (IIA ovular), conical ampulla (IIB), and a wide ampulla (WA) models with appropriate (3 mm) and oversized (5 mm) minimal ductal diameters (MDD) relative to our prototype's waist diameter (Figure 4.3). Dimensions of all simplified models are detailed in Table 4.1. The WA model simulates conditions in which the device struts do not contact the ampulla walls, as could occur shortly after occlusion [2]. The 6 mm waist of the NFC prototype is designed to be twice the diameter of the appropriate PDA MDD. Model MDDs were designed such that the prototypes would evaluate 2x and 1.2x oversizing to serve as a safety factor for clinician device sizing. Additionally, elliptical morphology dimensions were applied for the IIA ovular model to account for irregularly shaped PDAs that occur *in vivo* (personal communication: Sonya Gordon, DVM; Ashley Saunders, DVM).

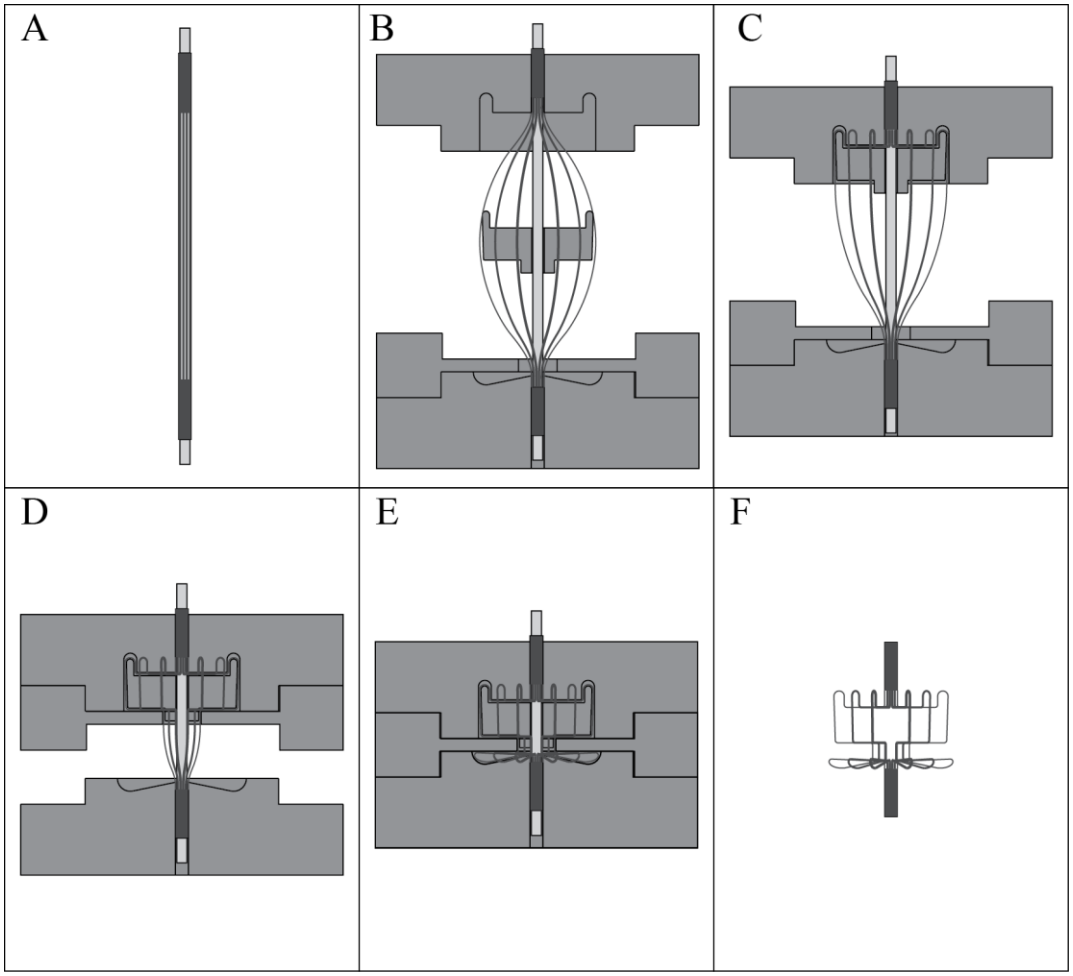

Figure 4.1: Shape setting procedure for NFC prototypes. A: Laser cut nitinol tube. Gauge pin placed within lumen across the length of the tube. B: Laser cut tube placed within shape setting clamps (top to bottom: proximal, waist, distal) with struts expanded to accommodate proximal spacer (top half of clamps not shown. Spacer shown sectioned in half). C: Proximal spacer placed within proximal clamp. D: Waist clamp butted against proximal clamp. E: Distal clamp butted against waist clamp. F: Shape set nitinol cage following heat treatment and removal from the fixture.

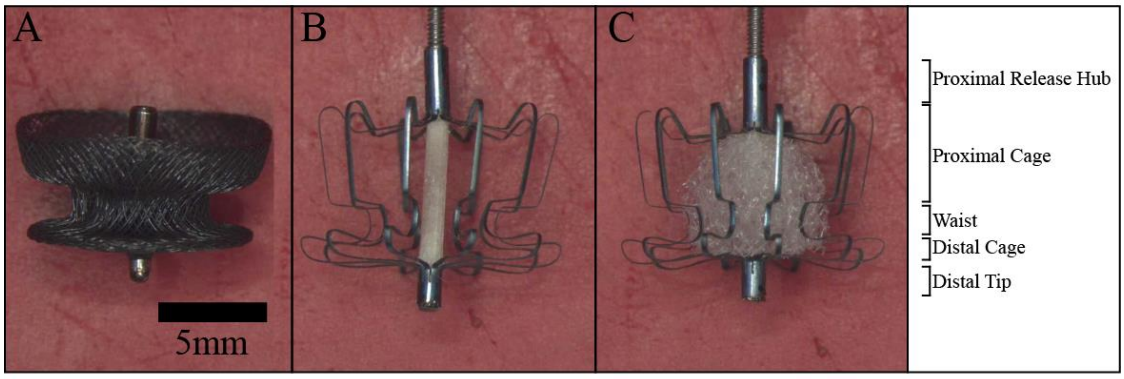

Figure 4.2: NFC prototype comparison to ACDO. A: ACDO, B: NFC with foam compressed, C: NFC with foam expanded. Cage regions defined in left most column.

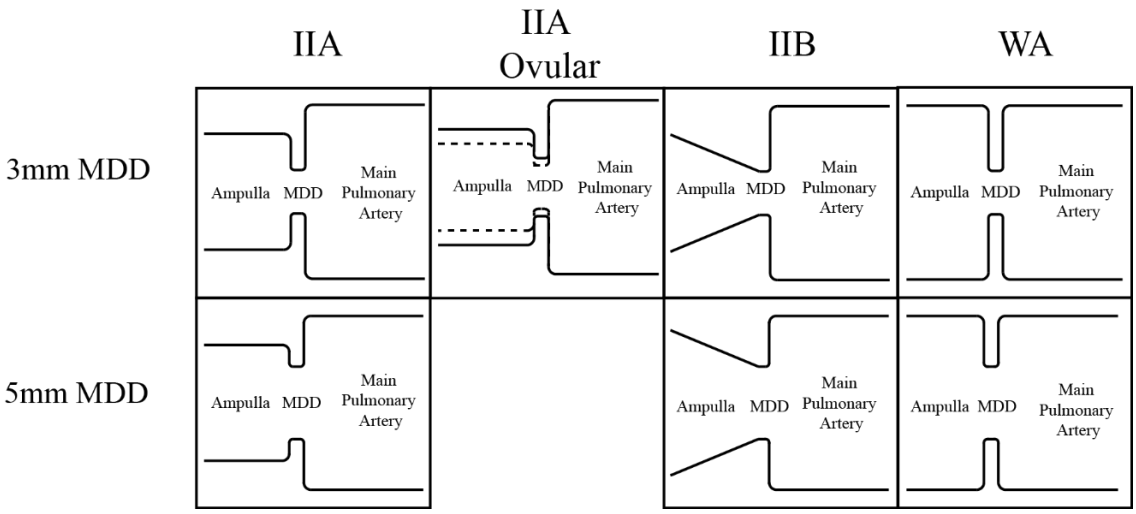

Figure 4.3: Simplified PDA geometries. Schematics of each simplified thin-walled PDA model used in experimental flow stability studies.

Table 4.1: Dimensions of simplified thin-walled PDA models used in experimental flow stability studies.

Model	Ampulla Diameter (mm)	Minimal Ductal Diameter (mm)	Device Waist Oversizing
IIA	8	3	2x
	8	5	1.2x
IIA ovular	6 x 8	3 x 4	~2x
IIB	10	3	2x
	10	5	1.2x
Wide Ampulla	12	3	2x
	12	5	1.2x

Flexible, thin-walled polydimethyl siloxane (PDMS) molds of the simplified PDA geometries were constructed by 3D printing the vessel lumen using a dissolvable material and the outer wall mold pieces using a non-dissolvable material. PDMS resin was injected into the mold to form a wall thickness of approximately 0.5 mm and then cured. The printed polymer lumen was then dissolved from the PDMS mold in a heated base bath solution completing the model.

Two rigid PDMS molds were constructed based on reconstructions from computed tomographic angiograms (CTA) of the canine PDA. The rigid physiological PDA models were made in a similar fashion as described in Wierzbicki et al. as the complex geometry complicates flexible, thin-walled mold manufacture. Briefly, the surfaces of the aorta, PDA, and, MPA were extracted and sectioned using Mimics (Materialise, Belgium). Because the CTAs provided were an unusual morphology, the geometry was minimally modified to resemble a the IIA and IIB taper with a 3 mm MDD (Figure 4.4). The extracted

volume was then 3D printed with a dissolvable material and the model was cast in PDMS in a similar manner to the simplified PDA models.

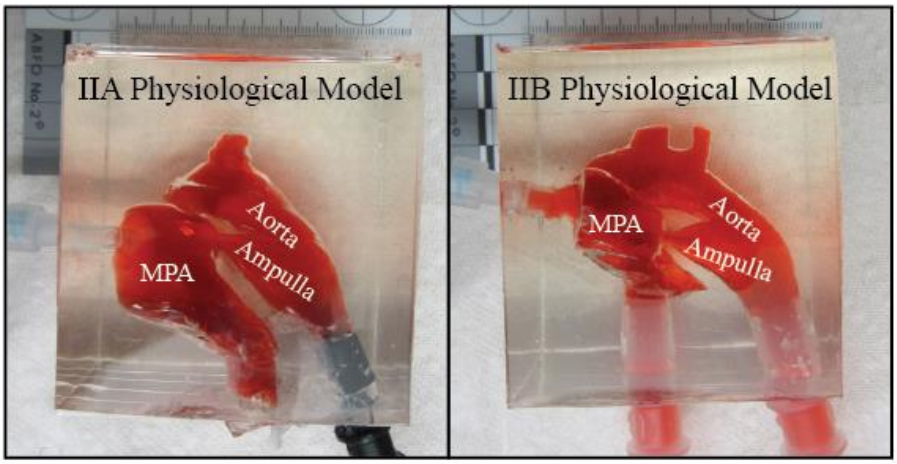

Figure 4.4: Physiological PDA models used to obtain feedback on deployment characteristics. Red dye placed within lumen for visibility of the aorta, ampulla, main pulmonary artery (MPA), and minimal ductal diameter (narrowest portion between ampulla and MPA).

4.2.3 Mechanical Verification Tests

4.2.3.1 Device Fatigue Test

A preliminary analysis of fatigue characteristics was conducted by axially cycling the nitinol frame on a dynamic mechanical analysis (DMA) unit (DMA Q800, TA instruments, New Castle, DE). Three untreated, NFC_{Tn}, and three electro-polished, NFC_{TkEP}, nitinol frames were cycled with an amplitude of 1 mm at a frequency of 2 Hz for approximately one million cycles simulating small deflections that the devices would

be subject to *in vivo*. Untreated samples were prepared as described in Section 2.1 and were not electropolished or processed further following shape setting. The force imparted by the NFC_{Tn} and NFC_{TkEP} devices were recorded and monitored for sudden changes and the struts were visually inspected for damage following the test.

4.2.3.2 Radial Force Measurements

The radial force exerted by the nitinol frames of the NFC_{Tn} and NFC_{Tk} and ACDO were measured using a Blockwise J-Crimp^{TM} RJA62 Radial Compression Station (Blockwise Engineering LLC, Tempe, AZ) attached to an Instron 5965 Test Frame (Instron, Norwood, MA) held at 37°C. The Blockwise utilizes a linear relationship between the axial force measured by the load cell (F), and the total radial force (TRF), as shown in equation (1):

$$TRF = 2.712 * F \qquad \text{Eq. (4.1)}$$

where, 2.712 is a conversion constant provided by Blockwise for our instrument.

Devices were first loaded into a polytetrafluorethylene (PTFE) sheath (1.35 mm ID, Cole Parmer, Vernon Hills, Il) and positioned within the bore of the Blockwise for delivery. The sheath was then retracted, allowing the devices to expand. Both distal and proximal cages contacted the straight tubular bore. The radial force of the NFC_{Tn}. NFC_{Tk}, and ACDO was measured at diameters between 4 and 12 mm within the bare surface bore of the Blockwise, denoted S_{Tn}, S_{Tk}, and S_{ACDO} respectively. Additionally, devices were deployed into a 5.5 mm ID, 6.5 mm OD vessel mimic (LifeLike Biotissuue, London, ON)

placed within the Blockwise bore to measure the constrictive force required to prevent full vessel distension resulting from the nitinol frame, denoted B_{Tn}, B_{Tk}, and B_{ACDO}.

As the NFC prototypes and ACDO exhibit a very different contact area, strut and constrictive force were not directly compared. Therefore, wall tension within the mock vessel was calculated to compare mechanical properties of the devices. The NFC radial forces (S_{Tn}, S_{Tk}) and blockwise radial constrictive forces (B_{Tn}, B_{Tk}) were divided by the ten total struts, to obtain the radial force per strut ($\mathbf{s}_{Tn}$, $\mathbf{s}_{Tk}$) and constrictive force per strut (b_{Tn}, b_{Tk}), respectively. By measuring these two forces, the wall tension as seen in the vessel due to the NFC prototypes can be calculated as,

$$\tau_{NFC} = \frac{\boldsymbol{s}_{NFC} - \boldsymbol{b}_{NFC}}{2L\cos\alpha}, \qquad \text{Eq (4.2)}$$

where, τ_{NFC} is the wall tension in the vessel imparted by an NFC device (N/mm), $\mathbf{s}_{NFC}$ is the radial force per strut (N), b_{NFC} is the constrictive force per strut (N) of the NFC_{Tn} or NFC_{Tk} prototypes, and L is the strut length contacting the vessel (mm). Figure 4.5 below illustrates the strut isolation and free body diagram for the calculation.

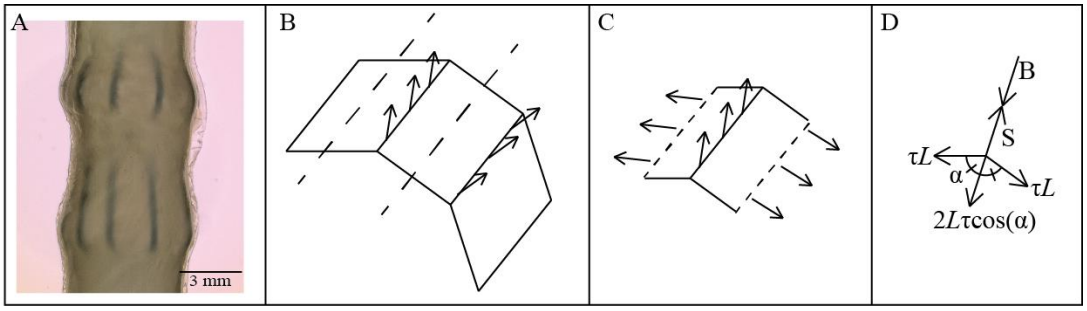

Figure 4.5: Illustration of vessel mimic wall tension calculation. A: NFC_{Tk} in mock vessel. Proximal (bottom) and distal (top) struts seen contacting the vessel wall. B: Section of idealized decahedron geometry formed by struts contacting the vessel wall. C: Vessel segment looking at only one strut. D: Free body diagram of strut contact point to analyze wall tension, τ.

As the ACDO is a continuous structure and does not have discrete struts, it was more appropriate to calculate wall tension as,

$$\tau_{ACDO} = (P_S - P_B)r, \qquad \text{Eq (4.3)}$$

where τ_{ACDO} is the wall tension generated by the ACDO, r is the radius of the bore diameter, P_S, the contact pressure applied by the ACDO, was calculated as,

$$P_S = \frac{S_{ACDO}}{SA_{contact}}, \qquad \text{Eq (4.4)}$$

and P_B, the compressive stress applied by the Blockwise to the ACDO within the mock vessel, was calculated as,

$$P_B = \frac{B_{ACDO}}{SA_{contact}}, \qquad \text{Eq (4.5)}$$

where, S_{ACDO} is the radial force (N) applied by the ACDO, and $SA_{contact}$ is the surface area (m^2) of the ACDO in contact with the vessel wall, and S_{AV} is the radial force (N) applied by the ACDO within the mock vessel. The strut contact length and $SA_{contact}$ were determined from images, similar to the one shown in Figure 4.5A, with Image-J™

software (http://rsb.info.bih.gov/ij/). Three NFC_{Tn} and NFC_{Tk} were measured, and one ACDO were tested, at least three times each at each diameter.

4.2.4 Device Stability Testing Using Simplified in vitro Models

4.2.4.1 Flow Setup for Simplified *in vitro* PDA Models

A gravity fed flow loop held at approximately 37°C was built to create a pressure driven flow to subject the devices to physiological (100 mmHg) and elevated (200 mmHg and 300 mmHg, respectively) pressures. A needle valve positioned upstream of the PDA model was used to control the pressure gradient applied to the system. Figure 4.6 displays a schematic of the flow set up.

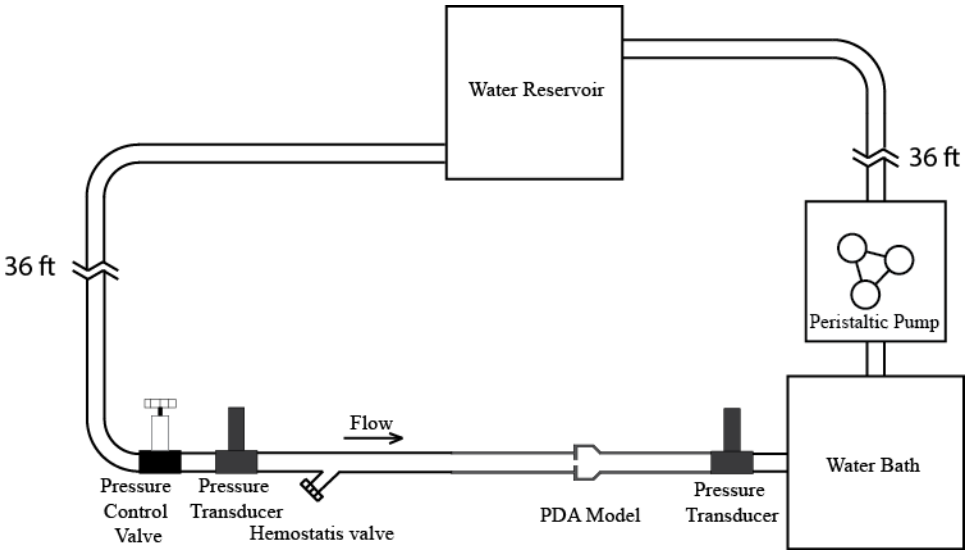

Figure 4.6: Schematic of flow loop used in device stability studies.

4.2.4.2 Device Preparation and Delivery

To provide a worst-case scenario for the NFC device geometry, the NFC_{Tn} prototypes were used for comparison against the commercial ACDO device, as nitinol frames with a wall thickness smaller than of 0.0015" would not be used for this application. The NFC_{Tn} prototypes were fitted with compressed SMP foams and loaded into PTFE introducer tubes. After setting the pressure gradient across the ductus to 100 mmHg, a 4 Fr sheath (Cook Medical, Bloomington, IN) was passed across the MDD such that the tip resided in the modeled pulmonary artery. The introducers containing devices were loaded into the sheath and the devices were advanced through the sheath until the distal cage was exposed. The delivery cable and sheath were retracted together such that the distal cage rested against the pulmonic ostium of the model. The proximal cage was then unsheathed. The delivery cable was then pushed forward to allow the proximal cage to conform to its cupped shape and to position the foam in the ampulla, MDD and pulmonary artery. Prior to release, a push-pull test was performed, in which gentle forward and backward motion was applied to the delivery cable to ensure that the device was stable and not easily pushed into the pulmonary artery [15]. The SMP foam was allowed to fully expand (~2 mins) before releasing the device by unscrewing it from the delivery cable.

4.2.43 Device Stability Tests

Three unique NFC_{Tn} prototypes and one 6 mm waist ACDO were tested in all simplified models three times each. The pressure gradient across the model was set to 100 mmHg prior to delivery of the devices. Both the NFC_{Tn} and ACDO were delivered into

the simplified PDA models following the protocol described in 2.4.2. Following device deployment, the pressure gradient was readjusted to 100 mmHg, as the pressure across the PDA increases following deployment, and held at 100, 200, and 300 mmHg for five minutes each consecutively, while images were captured in one minute intervals using a digital camcorder (Panasonic HDC-HS80, Newark, NJ). Devices in the all 3 mm and 3x4 mm MDD models were subjected to all three pressures, but the devices, when implanted into the 5 mm MDD models, were only subjected to 100 and 200 mmHg. The flow system could not develop a pressure gradient of 300 mmHg with devices (NFC or ACDO) deployed, as the devices did not generate a high enough resistance to flow. Following the tests, migration/dislocation of the distal tip, relative to the initial deployed position was measured using ImageJ™ software.

4.2.5 Deployment Performance in Physiological in vitro Models

4.2.5.1 Device Preparation and Delivery

NFC prototypes were fabricated using methods described in Section 2.1. The delivery characteristics of 6 mm NFC_{Tn} and NFC_{Tk} prototypes and a 6 mm ACDO were evaluated in the two different rigid PDMS models of a physiologically representative PDA as shown in Figure 4.4. Two NFC_{Tn} and NFC_{Tk} prototypes, and one ACDO were prepared and loaded into PTFE introducers. Before delivery, the pressure drop across the ductus was set to 120 mmHg, and the flow rate on the pump was constant for the entire test. The water in the flow loop was maintained at approximately 37°C. One of each type of NFC was deployed by a clinician into each physiological model, in a similar manner to that

described in Section 2.4.2 using fluoroscopic guidance. The same ACDO was used in both deliveries. Deployment characteristics such as ease of advancement through the catheter, deployment, positioning, and retraction were recorded.

While the pressure drop across the ductus was set to 120 mmHg, and the flow rate on the pump was constant for the entire test, the pressure gauges were not positioned immediately proximal and distal to the model ductus. Therefore, the actual pressure drop across the PDA may have presented lower than measured. However, the goal of this experiment was not to assess stability, as evaluated in Device Stability Testing (see Section 2.4), but rather to obtain clinician feedback on deployment characteristics and potential future improvements.

4.2.5.3 Device Retraction and Repositioning

Following deployment and after allowing the foam to fully expand, retraction was attempted by advancing the catheter to the proximal struts and pulling on the delivery cable and retracting them back into the sheath. Following recapture, the device was redeployed by the clinician following the previously described delivery protocol. Retraction and redelivery characteristics and clinician recommendations were recorded.

4.3 Results and Discussion

4.3.1 Device Fatigue

All six devices withstood the one million cycle fatigue test, assessing strut integrity. The NFC_{Tn} (n=3) and NFC_{TkEP} (n=3) devices produced a constant load of 0.019 ± 0.001 N and 0.013 ± 0.001 N, respectively, throughout the testing. Sharp decreases in the load would have indicated that a strut had completely fractured. There were no grossly visible fractured struts, on either the NFC_{Tn} or NFC_{TkEP}, indicating that the nitinol frames should withstand implantation even with minimal post processing done on the laser cut nitinol. The NFC_{TkEP} frames did feel more fragile and soft compared to the untreated samples when loading them into the DMA clamps. Additionally, the NFC_{TkEP} samples also exhibited lower force during fatigue testing and exhibited permanent elongation following fatigue testing, indicating that the treatment could have affected the material's strength. The lower force could also be attributed to the reduced strut width of the NFC_{TkEP} (0.009") compared to the strut width of the NFC_{Tn}, (0.011") [69].

Figure 4.7A-C shows a comparison of the NFC_{Tk} and NFC_{TkEP}, and an NFC_{TkEP} positioned within the DMA clamps. Figure 4.7D-F show SEM micrographs of NFC_{Tn} , NFC_{Tk}, and NFC_{TkEP} prototypes post-test. The strut thicknesses of the NFC_{Tn} and NFC_{Tk} prototypes appear much greater than that of NFC_{TkEP} sample due to the recast that formed on the edge during laser cutting because of melted nitinol. Additionally, minor defects or notches (Figure 4.7F) were present on some struts at the bends in the proximal and distal zones, but these were believed to either form during shape setting or as a defect during

laser cutting as the notches only on strut edges and were not present throughout the entire strut width. Further, defects did not propagate during fatigue tests.

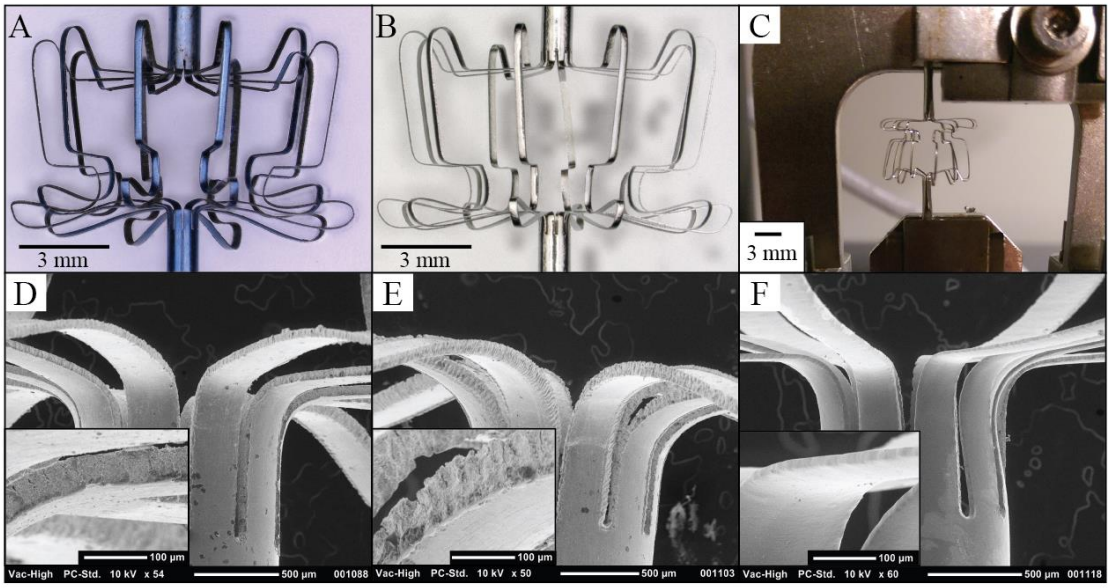

Figure 4.7: A: Untreated thick-walled, NFC_{Tk}, prototype. B: Electropolished thick-walled, NFC_{TkEP}, prototype. C: NFC_{TkEP} prototype loaded into DMA clamps for fatigue testing. D: SEM micrograph of untreated NFC_{Tn}. E: SEM micrograph of NFC_{Tk}. F: SEM micrograph of NFC_{TkEP}.

While optimization to the electropolishing step is still required, it was demonstrated that both NFC_{Tk} prototypes could be treated with a commercially relevant, light electropolish (~0.0006" total material removal) and untreated NFC_{Tn} prototypes could withstand a short-term fatigue test. Electropolishing is a standard and typically a necessary processing technique used on laser cut parts to improve surface finish, corrosion

resistance biocompatibility and fatigue life by reducing stress concentrations and heat affected zones [70-72]. Formation of recast, debris, and heat affected zones is a known issue related to laser cutting nitinol with long pulsed excimer lasers (100 Hz) [73]. Therefore, future nitinol frames should be cut using a femtosecond pulsed laser, to reduce these effects, in turn reducing standard processing techniques prior to electropolishing [70, 73].

This pilot fatigue test provided preliminary evaluation of frame integrity to ensure that the device would not fail on a short time scale with the proposed number of struts and strut width, which prompts further evaluation of the NFC_{Tn} design.

4.3.2 Radial Force Measurements

The contact pressure/strut force of the NFC_{Tn}, NFC_{Tk}, and ACDO device was plotted against bore diameter as shown in Figure 4.8A.1-A.3. The strut force of the NFC_{Tk} was higher than that of the NFC_{Tn} at all diameters tested, as expected. Contact pressure/strut force was highest for all devices in the smallest bore diameters and tended to decrease as the bore diameter increased, allowing the NFC cage diameter to increase, until the bore diameter was approximately the same diameter as the original NFC cage design. The large standard deviation in some tests is due to variations in handling during device deployment. Since the devices are delivered into a straight tube and not into the PDA geometry, as they are intended to fit, the cages would sometimes angle, torque, or struts would catch on themselves, influencing the measured forces. These effects would be minimized during delivery into physiological PDAs due to the different stages and

regions of cage deployment and delivery. Local maxima and minima in the curves are due to the unique recovery shapes of the multi-cage design expanding at different diameters.

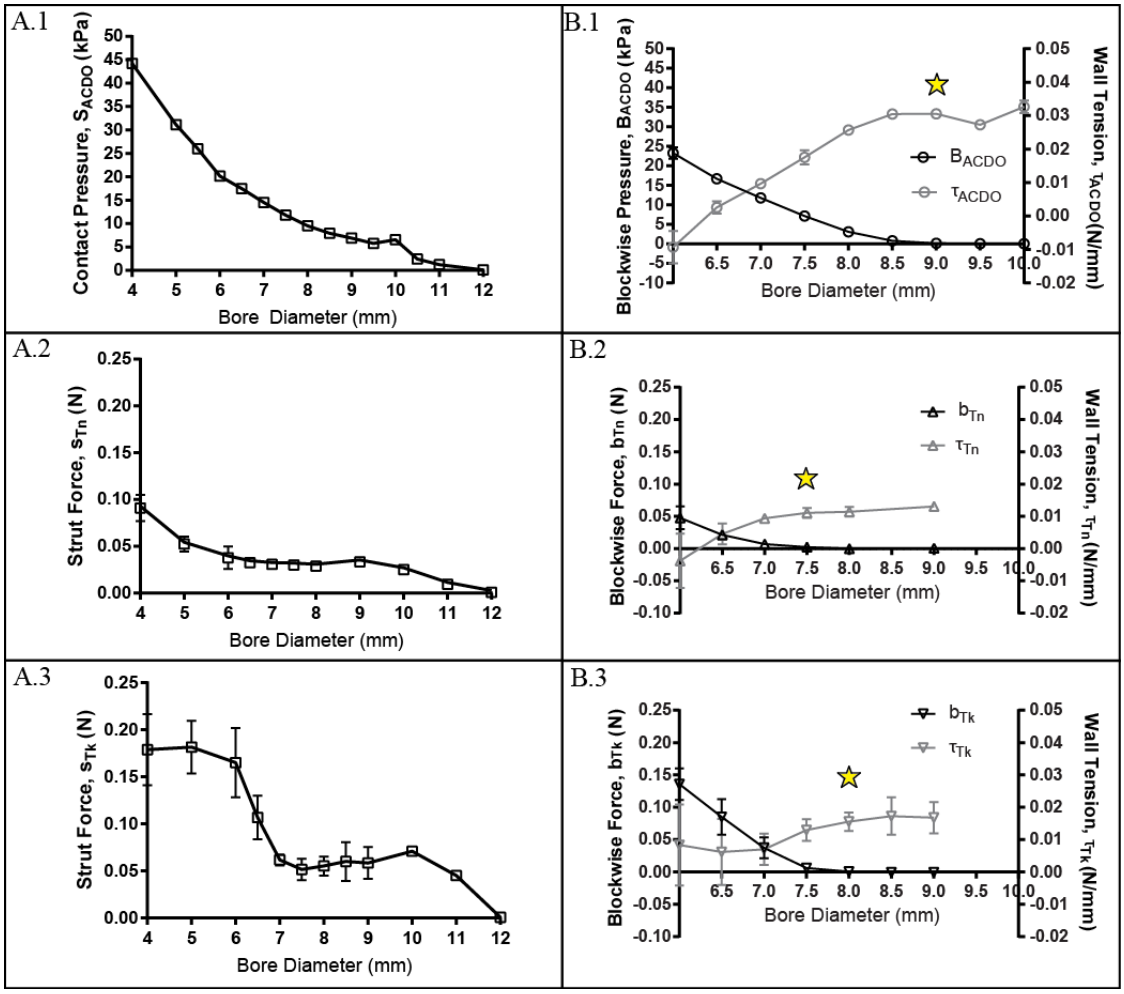

Figure 4.8: Strut force/contact pressure, Blockwise pressure/force and wall tension of ACDO, NFC_{Tn}, NFC_{Tk} devices. A.1-A.3: Contact pressure/strut force of the ACDO, NFC_{Tn}, NFC_{Tk} respectively. B.1-B.3: Blockwise pressure/force and wall tension of the ACDO, NFC_{Tn}, NFC_{Tk} respectively. Three NFC_{Tn} and NFC_{Tk} and one ACDO were tested at least three times each at each Blockwise bore diameter.

The plots in Figure 4.8B.1-B.3 display the compressive force applied by the Blockwise blades (B_{ACDO}, b_{tn}, b_{tk}) that prevented device expansion within the vessel mimic and the wall tension generated within the vessel wall due to device expansion (S_{ACDO}, $\mathbf{s}_{tn}$, $\mathbf{s}_{tk}$). At smaller bore diameters, the Blockwise applies a compressive force, preventing device cage expansion, and the wall tension (τ_{ACDO}, τ_{Tn}, τ_{Tk}) is low at smaller bore diameters as the Blockwise is taking most the load. However, as the bore diameter increases, the strength of the vessel wall matches the radial force imparted by the device cage, creating a stress equilibrium between the vessel mimic and device (Figure 4.8B.1-B.3, starred region). At this point, maximum vessel distension has occurred and the Blockwise compressive force approaches zero. While it is difficult to compare strut force and contact pressure between the NFCs and ACDO due to differences in geometry, wall tension that developed due to device expansion can be compared. Table 4.2 shows the wall tension and vessel distension, the difference between the bore diameter at stress equilibrium and the vessel OD. The ACDO generated 0.031 ± 0.0007 N/mm of wall tension compared to 0.009 ± 0.0007 and 0.012 ± 0.0034 N/mm generated by the NFC_{Tn} and NFC_{Tk}, respectively.

Table 4.2: Vessel mimic distension for each device type defined as the difference between the bore diameter at equilibrium and the unloaded vessel mimic OD.

Device Type	Wall Tension at Stress Equilibrium (N/mm)	Approximate Vessel Distension at Stress Equilibrium (mm)
ACDO	0.031 ± 0.0007	3
NFC_{Tn}	0.009 ± 0.0007	1
NFC_{Tk}	0.012 ± 0.0034	1.5

The distension of both the NFC_{Tn} and NFC_{Tk} prototypes and ACDO was approximately 1, 1.5, and 3 mm, respectively. While the large amount of vessel distention in all devices could lead to clinical concerns such as vessel perforation, or pressure necrosis, there has not been clinical evidence of such incidence due to oversizing in stenting [69] or PDA procedures in literature. While there have not been reported incidences of vessel perforation using the ACDO, clinicians have expressed concerns on the amount of over sizing in the ampulla in some cases [personal communication, Sonya G. Gordon DVM]. However, animal studies have shown that stents can protrude as much as 2 mm further than the adventitia and remain covered with connective tissue [69]. Overall, the similar deployment characteristics of the NFC_{Tk} along with lower distension (2x lower) and wall tension (2.5x lower) encourage further investigation. The lower vessel distension and reduced wall tension generated by the NFC prototypes indicate that

implantations of this device should not result in significant vessel trauma or ampulla rupture.

It should be noted that the radial force values measured include contributions of both the proximal and distal cages representing a worst-case deployment wherein the entire device was deployed into a straight tubular, Type III (geometry not shown) PDA [7]. In a standard deployment, only the proximal cage and waist apply outward forces to the ductus. The distal cage resides along the pulmonary artery wall and therefore should not exert an outward force on the vessel. However, it was not possible to replicate this due to the straight, cylindrical geometry of the Blockwise, meaning the radial force may be slightly overestimated for all devices including the ACDO.

4.3.3 Device Migration in Simplified in vitro Models

Migration was measured as movement of the distal tip of the device relative to the deployed position for stability evaluation. Qualitative inspection of the images captured of the devices deployed into the 3 and 5 mm MDD models (Figures 4.9 and 4.10 respectively) do not show motion of either the NFC_{Tn} or ACDO frames. However, measurements of distal tip motion displayed minimal movement of both the NFC_{Tn} and ACDO. The device migration in the 3 mm MDD models (2x oversized MDD) was lower or comparable to the devices deployed into the 5 mm MDD (1.2x) sized models, with values shown in Table 4.3. The axial migration of the NFC_{Tn} prototype, when compared to the ACDO is negligible. The greatest migration occurred at a pressure gradient of 300 mmHg in the simplified IIA 3mm and WA 3mm models for both the NFC_{Tn} and ACDO

configurations. Zero migration indicates that either there was no motion seen, or that the distal nub retracted towards the minimal ductal diameter. The retraction occurs in response to the ampulla widening and allowing the proximal and waist portion of the cage to more fully recover to their unconstrained shape.

Device migration occurred in response to flow passing through and compressing the foam into the distal cage, elongating the cage, but not dislodging the frame. Since device migration was measured as the axial motion of the distal cage, the foam compression could exaggerate skew the migration measurements such that we measure the cage elongation and not actual dislocation of the prototype through the anatomy.

A secondary result of the foam compression was partial collapse of the proximal cage. The drag imparted on the foam that caused elongation of the distal cage also pulled the attached proximal nub toward the MDD. Proximal cage collapse was most pronounced in the 3 mm IIA and IIB models (Figure 4.9). However, the compression may not be as pronounced when implanted *in vivo* as flow across the device will be negligible following foam embolization. Standard delivery practices of the ACDO indicate that the device should not be released from the delivery cable until only a minor persistent flow through the ductus is present or it is completely occluded [33], thereby minimizing compression and migration due to flow.

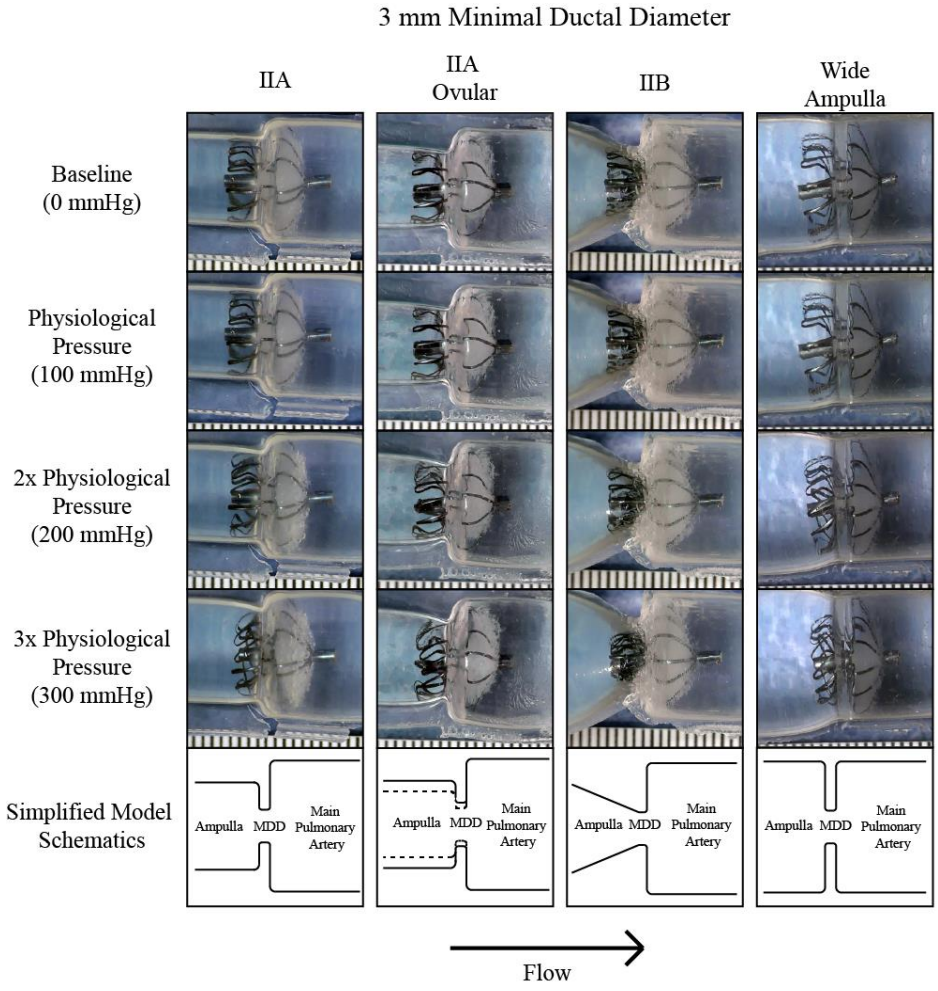

Figure 4.9: Dislocation study for 3 mm MDD simplified models. NFC_{Tn} prototypes deployed in all 3 mm MDD PDA geometries at increasing pressures (top to bottom). Simplified schematic of each model shown in the bottom row. Minor motion of the distal tip (pulmonary artery side) is present in all models. Proximal cage collapse is apparent at a pressure gradient of 200 mmHg and above.

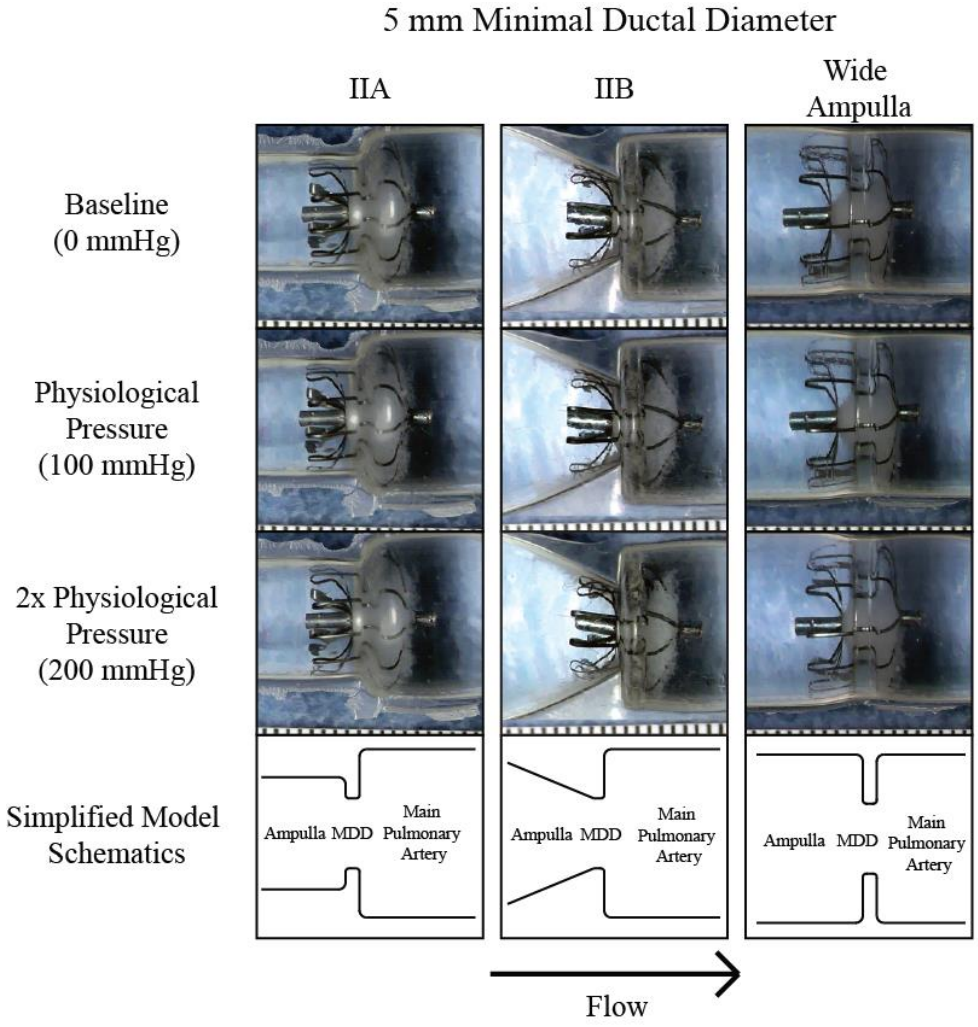

Figure 4.10: Dislocation study for 5 mm MDD simplified models. NFC$_{Tn}$ prototypes deployed in all 5 mm MDD PDA geometries at increasing pressures (top to bottom). Negligible motion of the distal tip is present. Simplified schematic of each model shown in the bottom row. Proximal cage compression is not as apparent, as the larger MDD afforded less resistance to flow.

Table 4.3: NFC_{Tn} and ACDO migration in simplified, flexible PDA models.

	NFC_{Tn} Axial Migration (mm)			ACDO Axial Migration (mm)		
	100 mmHg	200 mmHg	300 mmHg	100 mmHg	200 mmHg	300 mmHg
IIA 3mm	0 ± 0.1	0.1 ± 0.1	0.5 ± 0.3	0 ± 0.1	0.06 ± 0.4	0.1 ± 0.3
IIA 3x4mm	0 ± 0.2	0.1 ± 0.3	0.2 ± 0.4	0 ± 0.1	0.1 ±0.2	0.4 ± 0.1
IIB 3mm	0 ± 0.7	0.1 ± 0.1	0.1 ± 0.2	0.02 ± 0.03	0.1 ± 0.1	0.1 ± 0.15
WA 3mm	0 ± 0.1	0.2 ± 0.2	0.6 ± 0.2	0 ± 0.1	0.2 ± 0.3	0.4 ± 0.4
IIA 5mm	0.06 ± 0.1	0 ± 0.3	n/a	0.1 ± 0.2	0 ± 0.2	n/a
IIB 5mm	0 ± 0.2	0 ± 0.2	n/a	0.1 ± 0.1	0.1 ± 0.2	n/a
WA 5mm	0.1 ± 0.1	0.2 ± 0.2	n/a	0.031 ± 0.1	0.1 ± 0.2	n/a

It is promising that the NFC_{Tn} prototypes, even with an oversize factor of only 1.2x, remained stable at up to twice the physiological pressure, despite clinical recommendations for devices be with a waist 2x oversized relative to the MDD. Additionally, two-dimensional angiography of the PDA does not always result in an accurate MDD measurement and therefore it is important that a safety factor is incorporated into the device sizing. Whereas, the simplified models exhibited a rigid MDD, the flexible nature of the canine PDA may allow the struts in the waist to more fully expand, allowing the device to more closely return to its programmed shape. Greater expansion of the waist will result in frame conformance similar to that seen in the oversized MDD models, reducing the prototype's protrusion into the pulmonary artery and minimizing the effects of foam compression. While the flexible, thin-walled PDMS

models did not allow for extensive MDD dilation, minimal NFC migration in the oversized MDD's demonstrated that the device could withstand a vessel configuration which may occur after deployment.

Overall, the minimal measured migration of the NFC_{Tn} prototypes is comparable to that of the ACDO in all models tested at physiological and elevated pressures. The test shows that there is a minimal risk of NFC device migration following implantation.

4.3.4 Device Deployment and Retraction in Physiological in vitro Models

4.3.4.1 Device Deployment and Retraction Characteristics

The NFC_{Tk} and NFC_{Tn} prototypes and ACDO were successfully delivered to both IIA and IIB physiological models. The angle at which the models were deployed as well as the rigid nature of the model did not allow the proximal cages of any NFC devices or the ACDO to return and hold their preformed shape and conform to the ampulla taper as expected in the elastic PDA vessel of a dog. Figure 4.11, below shows the deployment sequence of an NFC_{Tk} deployed into the IIB Model.

Retraction was successful in all device types (NFC_{Tn}, NFC_{Tk}, ACDO) tested. For each device, the sheath was positioned against the proximal struts and pulling on the delivery cable. For the NFC_{Tn} and NFC_{Tk} prototypes, retraction was attempted after the foam had expanded (~2-5 mins). The force required to retract the NFC_{Tk} was comparable to that of the ACDO.

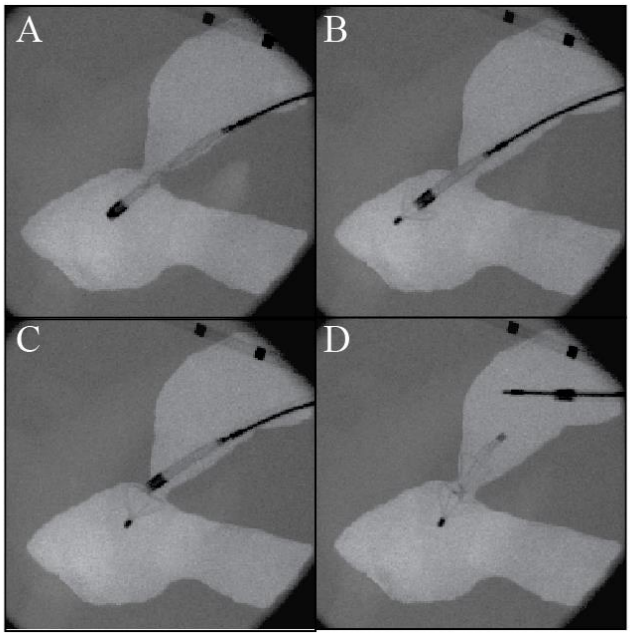

Figure 4.11: Delivery sequence of NFC_{Tk} in physiological IIB model. A: Sheath deployed across the MDD. The compressed NFC can be seen within the sheath. B: Distal cage deployed. C: Distal cage pulled against pulmonary artery ostium. D: Proximal cage deployed and device released. Mask overlayed to emphasize PDA morphology.

4.3.4.1.1 Clinician Feedback on Thin-Walled NFC Device Characteristics

The NFC_{Tn} was successfully deployed, retracted, and repositioned, and passed a light push/pull test performed by a clinician (Sonya G Gordon, DVM). However, there were some concerns regarding the tactile feedback during delivery as well as visibility under fluoroscopy. First, the NFC_{Tn} was more difficult to distinguish under fluoroscopy compared to the NFC_{Tk} or the ACDO (Figure 4.12). This lack of strut opacity forced the clinician to rely mostly on the radiopaque markers located on the proximal and distal tips during placement. Secondly, during deployment of the distal cages, clinicians typically

feel for a distinct “pop” as the distal cage of the ACDO is advanced out of the cage and abruptly expands to its preformed shape. The NFC_{Tn} exhibited a slight “pop”, but it was much less distinct as compared to the ACDO and NFC_{Tk} prototype deployment. Additionally, the distal cage of the NFC_{Tn} was easily deformed and did not provide a noticeable change in resistance to the clinician to indicate that the cage had caught onto the pulmonary artery wall. The proximal cage did not return to its programmed cup shape. Finally, following delivery of the proximal cage, it was relatively easy to push the frame through the ductus. It was noted that this lack of tactile feedback during deployment may make the NFC_{Tn} prototype delivery too different from the current ACDO, which may delay or inhibit device adoption. However, it is believed that these issues are related to the thin struts and increasing their thickness and respective stiffness, could improve these qualities.

4.3.4.1.2 Clinician Feedback on Thick-Walled NFC Device Characteristics

The NFC_{Tk} prototype was successfully deployed, retracted, and repositioned, and passed a heavy push/pull test in which the clinician applied much more force than what is used in normal canine deliveries. The increased strut wall thickness for NFC_{Tk} (0.002”) compared to the NFC_{Tn} (0.0015”) greatly improved the overall feel and visibility of the device under fluoroscopy (Figures 4.12). Further, the NFC_{Tk} strut thickness did offer more resistance than the NFC_{Tn} while advancing through the catheter, but it was still less than the ACDO, and was not an issue. The distal cage of the NFC_{Tk} exhibited a distinct “pop” when it was deployed and offered noticeably higher resistance compared to the NFC_{Tn} prototype when pulled against the pulmonic ostium of the MDD, indicating to the clinician

that it was in proper position and the proximal cage should be unsheathed. Like the NFC_{Tk}, the proximal cage of the NFC_{Tk} did not return to its programmed cupped shape. It was noted that this prototype "felt very nice coming out [of the sheath]" meaning that the clinician could feel the cages deploy and when they were in proper position. In summary, the increased tactile feedback and greater stiffness provided by the NFC_{Tk} prototype increases its ease of delivery compared to the NFC_{Tn} device.

4.3.4.1.3 Clinician Feedback on ACDO Characteristics

The ACDO was successfully deployed, retracted, and repositioned in the models. It offered the most resistance while advancing through the sheath, even compared to the NFC_{Tk}. The proximal cage of the ACDO did not return to its preformed shape and looked nearly identical to that of the NFC_{Tk}. This indicated that all devices (ACDO and NFC) were either oversized relative to the ampulla of the model, or more likely, the rigid model prevented ampulla distention and expansion, preventing return to their cupped geometries. In the future, flexible PDA models using the physiological anatomies should be created to more accurately mimic the deployment characteristics.

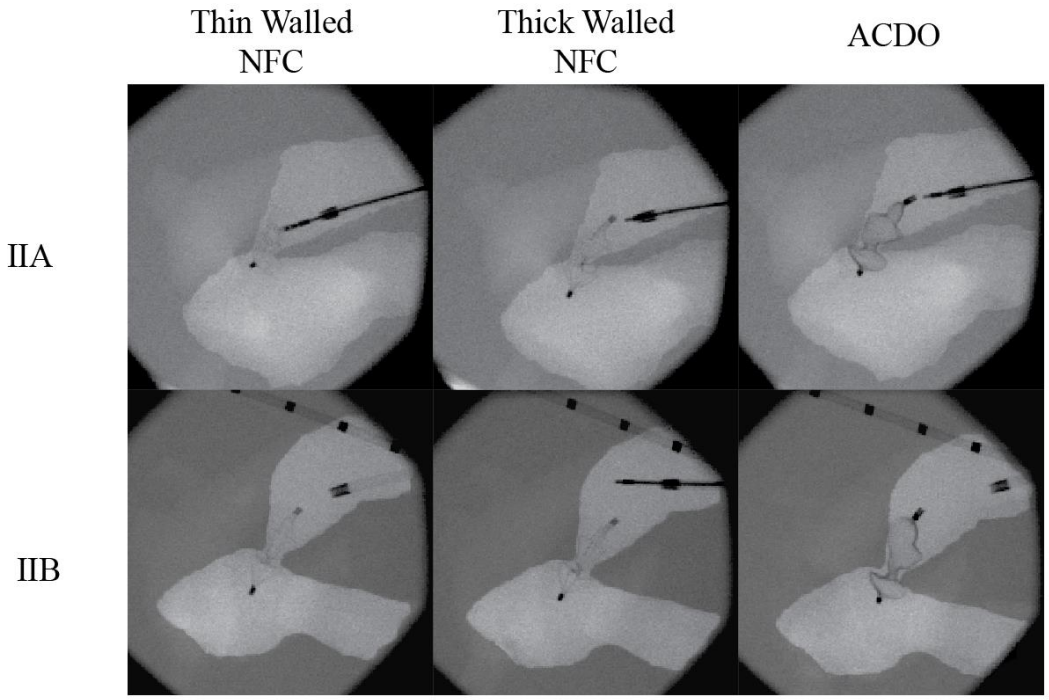

Figure 4.12: Devices deployed into physiological PDA models. A-C: Thin walled (NFC_{Tn}) NFC (still attached to delivery cable), thick walled (NFC_{Tk}) NFC, and ACDO (left to right) deployed into the IIA physiological model, respectively. D-F: NFC_{Tn}, NFC_{Tk}, and ACDO (left to right) fully deployed into the IIB physiological model, respectively.

4.5 Conclusions

While the ACDO is effective at treating canine PDA, it's large delivery system profile can be limiting when treating smaller dogs with narrow vasculature. The dense nitinol mesh of the ACDO is used for both stability and occlusion, whereas in the NFC nitinol is used for stability and an SMP foam is used for occlusion. The reduction in materials of the NFC prototypes has multiple benefits including improvement in ease of delivery by reducing both the force required to advance the device through the catheter

and having an equivalent force required to retract the device into the sheath, and potentially reducing the cost of production.

The NFC prototypes conformed to all design criteria. An interesting aspect of this design is the scalable nature of the prototype. Like the previous version of the prototype, the frame is scalable in that by changing the length of the laser cut struts, the diameter of the cages can be increased or decreased. As the delivery profile of the NFC is determined by the OD of the nitinol tube and compressed SMP foam, we predict that larger waist diameter NFCs can be delivered into smaller catheters and sheaths compared to comparable waist ACDOs. Additionally, by reducing the OD of the nitinol tubing used to create the frame, NFCs with a waist of 4 mm and smaller may be able to be delivered through a 4 Fr catheter (~1 mm ID). Figure 4.13 shows conceptual 4 mm and 8 mm waist NFC devices alongside the tested 6 mm waist NFC prototype.

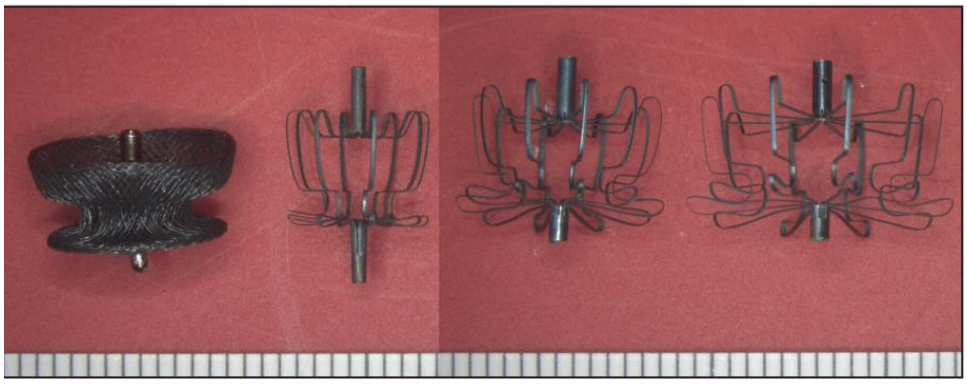

Figure 4.13: NFC device sizes compared to 6 mm ACDO. Left to right: 6 mm ACDO, 4 mm NFC (0.035” OD x 0.031” ID tubing), 6 mm NFC (0.044” OD x 0.040” ID tubing), 8 mm NFC (0.044” OD x 0.040” ID tubing).

Based on the supporting stability and deployment results for the NFC devices, we plan to pursue the NFC_{Tk} design in future studies due to the positive clinician feedback to its performance and familiar feel. The increased strut thickness should not negatively impact device stability or increase migration, and may improve these aspects by further resisting compression. With these changes to the strut thickness, and the positive results from the presented studies, including acute strut integrity, lower generated wall tension, minimal device migration, and positive clinician feedback, it is believed that the NFC could be used to treat canine PDA.

CHAPTER V

CONCLUSIONS

5.1 Summary

A shape memory polymer based nitinol foam cage (NFC) patent ductus arteriosus occlusion prototype device was designed, developed, and tested. The prototypes developed in this dissertation serve as a platform for the further development of a shape memory polymer based patent ductus arteriosus occlusion device. Both iterations of the prototype adhered to the design requirements: were deliverable and retractable into a 4 Fr sheath, were stable at physiological and elevated pressures, employed a simple detachment, and were visible under fluoroscopy.

A first generation NFC was constructed using a monolithic nitinol frame with two distinct cages and an SMP foam in the proximal cage. The prototype performed acceptably and conformed to the defined design requirements in the removal force, radial pressure, and *in vitro* stability tests. While successful, it was determined from these tests that device migration could be further reduced with nitinol frame refinement.

After compiling input from the clinician as well as investigating different configurations, a second generation NFC was developed which addressed the above limitations. Stability was improved to approximately match that seen with the ACDO by using a single nitinol cage with three distinct portions to better conform to the PDA anatomy. Additionally, the single, continuous cage gave the frame a propensity to compress around the MDD, similar to the mechanism of the ACDO, reducing the

possibility of dislocation. The second generation NFC prototypes conformed to the set design requirements and performed comparably to the ACDO in the radial force and stability tests. Expansion of the NFC produced lower wall tension at stress equilibrium in the vessel mimic compared to the ACDO, indicating that the NFC minimizes the risk of ampulla rupture or significant vessel trauma upon implantation of the device.

A unique feature of this design is the scalable nature of the prototype. The nitinol frame of both, first and second generation NFC prototypes can be scaled up or down to fit different sized PDAs by increasing or decreasing the length of the laser cut nitinol struts and shape set with different fixturing. Additionally, larger or smaller SMP foam cylinders can be placed within the frame, and the pore size and composition can be specifically tailored to allow for reduced compressed diameters or tailored actuation times. The compressed diameter of the NFC is only limited by either the outer diameter of the nitinol tube or compressed diameter of the SMP foam. Due to the reasons listed, we believe that small waist diameter (4 mm and smaller) NFCs can be made deliverable through 4Fr catheters (<1 mm ID) and larger devices can be delivered through smaller sheaths compared to the ACDO.

A series of polyacrylamide hydrogel-clotted SMP foams were fabricated and their modulus was measured in attempt to match that of blood-clotted small and large pore foams. Hydrogel-clotted foams with a modulus that most closely matched that of the blood-clotted foams were used in a verification test to demonstrate the utility of these materials. The dislocation force of the NFC was measured in multiple PDA geometries using bare foam and hydrogel-clotted foams and compared to the ACDO. While there was

minimal difference in the dislocation force between bare and hydrogel-clotted foams due to foam location within the nitinol frame, the low dislocation force of the NFC suggested that a stiffer device may be desired for ease of positioning. This hydrogel clot mimic developed serves as a useful tool in benchtop studies for future experiments. Currently, most device performance on the benchtop is performed using bare foams. However, this metric only estimates acute performance during delivery and shortly after deployment. Stability tests can and have been performed in this configuration, but the devices may perform differently clotted and in the past, the only way to measure these properties has been using actual blood clots or in *in vivo* studies. The utility of these materials is especially present in the testing of peripheral, PDA, and other high flow vessel occlusion indications to test a device's occlusion efficacy and ability to restore flow and pressures to surrounding vasculature.

5.2 Challenges and Future Directions

The goal of this project was to develop a prototype that was ready to be evaluated in an animal study and eventually commercialized. However, while many performance aspects were solved and evaluated in this work, additional testing is required prior to an *in vivo* study, including: nitinol tubing thickness optimization, laser cutting improvements, nitinol passivation, and corrosion testing.

First, thin wall walled (0.0015" wall thickness) devices were used for most of this work and they performed acceptably in all our verification tests, however it was indicated in our physiological deliveries that the thick walled (0.002" wall thickness) prototypes

exhibited a better feel and stability during deployment. As such, further testing involving these thicker walled devices needs to be investigated, including determining whether the struts of the thicker walled devices can still be shaped into the tight radius forms of the desired geometry, and ensuring that stability at physiological pressures is not impacted.

The prototypes evaluated in this work were fabricated in house using an excimer laser, due to expense and ability to rapidly iterate on the design. However, the excimer laser wavelength and pulse width are not optimized for cutting nitinol as these conditions tend to result in heat affected zones and recast around the cut edge, increasing the amount of post-processing required to improve the finish. Future devices should be fabricated using a femtosecond pulsed IR laser. The short pulses result in an athermal process which minimizes recast and heat affected zones, reducing the amount of post-processing required to prepare an implant grade finish device. It is believed that the light electropolish used in Chapter IV on femtosecond laser cut nitinol would result in an acceptable finish for implantation.

Laser cut nitinol devices must be passivated prior to implantation to reduce the amount of nickel on the surface of the material. This is typically done through electropolishing, a process that removes material from the surface and leaves a passive titanium dioxide surface layer improving biocompatibility and corrosion resistance. Because our devices form a complex geometry, multiple iterations of electropolish parameters may be necessary to ensure consistent and repeatable material removal across the entire device frame. Corrosion testing of the electropolished samples will need to be conducted to ensure that the treatment adequately passivated the surface.

Finally, 6 mm waist devices were the focus of the studies discussed within this work. Since PDAs come in wide range of sizes, different sized cages will need to be fabricated and tested. Currently, 4mm and 8mm waist devices have been prototyped, but more thorough testing of these sizes is required to ensure satisfactory performance.

REFERENCES

1. Nguyenba, T.P. and A.H. Tobias, *Minimally invasive per-catheter patent ductus arteriosus occlusion in dogs using a prototype duct occluder.* Journal of Veterinary Internal Medicine, 2008. **22**(1): p. 129-134.

2. Achen, S.E., M.W. Miller, S.G. Gordon, A.B. Saunders, R.M. Roland, et al., *Transarterial ductal occlusion with the Amplatzer vascular plug in 31 dogs.* Journal of Veterinary Internal Medicine, 2008. **22**(6): p. 1348-1352.

3. Eyster, G.E., Eyster, J. T., Cords, G.B., Johnston, J., *Patent ductus arteriosus in the dog: Characteristics of occurrence and results of surgery in one hundred consecutive cases.* Journal of the American Veterinary Medical Association, 1976. **168**(5): p. 435-438.

4. Patterson, D.F., *Epidemiologic and genetic studies of congenital heart disease in the dog.* Circulation Research, 1968. **23**(2): p. 171-202.

5. Singh, M.K., M.D. Kittleson, P.H. Kass, and L.G. Griffiths, *Occlusion devices and approaches in canine patent ductus arteriosus: Comparison of outcomes.* Journal of Veterinary Internal Medicine, 2012. **26**(1): p. 85-92.

6. Tobias, A.H. and C.D. Stauthammer, *Minimally invasive per-catheter occlusion and dilation procedures for congenital cardiovascular abnormalities in dogs.* Veterinary Clinics of North America-Small Animal Practice, 2010. **40**(4): p. 581-603.

7. Miller, M.W., S.G. Gordon, A.B. Saunders, W.G. Arsenault, K.M. Meurs, et al., *Angiographic classification of patent ductus arteriosus morphology in the dog.* Journal of Veterinary Cardiology, 2006. **8**(2): p. 109-114.

8. Saunders, A.B., M.W. Miller, S.G. Gordon, and A. Bahr, *Echocardiographic and angiographic comparison of ductal dimensions in dogs with patent ductus arteriosus.* Journal of Veterinary Internal Medicine, 2007. **21**(1): p. 68-75.

9. Gordon, S.G. and M.W. Miller, *Transarterial coil embolization for canine patent ductus arteriosus occlusion.* Clinical Techniques in Small Animal Practice, 2005. **20**(3): p. 196-202.

10. O'Sullivan, L., *Minimally invasive interventional cardiology: Diagnosis and transcatheter correction of patent ductus arteriosus in dogs.* Small Animal Veterinary Rounds, 2012. **1**(4): p. 1-4.

11. Stokhof, A.A., N. Sreeram, and W.T.C. Wolvekamp, *Transcatheter closure of patent ductus arteriosus using occluding spring coils.* Journal of Veterinary Internal Medicine, 2000. **14**(4): p. 452-455.

12. Saunders, A.B., S.E. Achen, S.G. Gordon, and M.W. Miller, *Utility of transesophageal echocardiography for transcatheter occlusion of patent ductus arteriosus in dogs: Influence on the decision-making process.* Journal of Veterinary Internal Medicine, 2010. **24**(6): p. 1407-1413.

13. Kittleson, M.D., *Patent ductus arteriosus*, in *Small animal cardiovascular medicine*. 1998, Mosby, Inc: St. Louis, MO. p. 218-230.

14. Franks, J.N., *Patent ductus arteriosus*, in *Small animal surgery secrets (second edition)*, J. Harari, Editor. 2004, Hanley & Belfus: Philadelphia, PA. p. 120-124.

15. Gordon, S.G., A.B. Saunders, S.E. Achen, R.M. Roland, L.T. Drourr, et al., *Transarterial ductal occlusion using the Amplatz® canine duct occluder in 40 dogs.* Journal of Veterinary Cardiology, 2010. **12**(2): p. 85-92.

16. Stanley, B.J., V. Luis-Fuentes, and P.G.G. Darke, *Comparison of the incidence of residual shunting between two surgical techniques used for ligation of patent ductus arteriosus in the dog.* Veterinary Surgery, 2003. **32**(3): p. 231-237.

17. Bureau, S.P., E. Monnet, and E.C. Orton, *Evaluation of survival rate and prognostic indicators for surgical treatment of left-to-right patent ductus arteriosus in dogs: 52 cases (1995-2003).* Journal of the American Veterinary Medical Association, 2005. **227**(11): p. 1794-1799.

18. Goodrich, K.R., A.E. Kyles, P.H. Kass, and F. Campbell, *Retrospective comparison of surgical ligation and transarterial catheter occlusion for treatment of patent ductus arteriosus in two hundred and four dogs (1993-2003).* Veterinary Surgery, 2007. **36**(1): p. 43-49.

19. Van Israel, N., A.T. French, J. Dukes-McEwan, and B.M. Corcoran, *Review of left-to-right shunting patent ductus arteriosus and short term outcome in 98 dogs.* Journal of Small Animal Practice, 2002. **43**(9): p. 395-400.

20. Miller, M., K. Meurs, and A. Boswood. *Echocardiographic assessment of PDA after occlusion (abstract)*. In *Proceedings of the 14th Annual Veterinary Medical Forum,* ACVIM. 1994. San Francisco, CA. p. 305-306.

21. Glaus, T.M., F. Berger, F.W. Ammann, W. Kiowski, S. Ohlert, et al., *Closure of large patent ductus arteriosus with a self-expanding duct occluder in two dogs.* Journal of Small Animal Practice, 2002. **43**(12): p. 547-550.

22. Sisson, D., *Use of a self-expanding occluding stent for nonsurgical closure of patent ductus arteriosus in dogs.* Journal of the American Veterinary Medical Association, 2003. **223**(7): p. 999-1005.

23. Hogan, D.F., H.W. Green, S. Gordon, and M.W. Miller, *Transarterial coil embolization of patent ductus arteriosus in small dogs with 0.025-inch vascular occlusion coils: 10 cases.* Journal of Veterinary Internal Medicine, 2004. **18**(3): p. 325-329.

24. Campbell, F.E., W.P. Thomas, S.J. Miller, D. Berger, and M.D. Kittleson, *Immediate and late outcomes of transarterial coil occlusion of patent ductus arteriosus in dogs.* Journal of Veterinary Internal Medicine, 2006. **20**(1): p. 83-96.

25. Hogan, D.F., H.W. Green, and R.A. Sanders, *Transcatheter closure of patent ductus arteriosus in a dog with a peripheral vascular occlusion device.* Journal of Veterinary Cardiology, 2006. **8**(2): p. 139-143.

26. Smith, P.J. and M.W.S. Martin, *Transcatheter embolisation of patent ductus arteriosus using an Amplatzer vascular plug in six dogs.* Journal of Small Animal Practice, 2007. **48**(2): p. 80-86.

27. Tanaka, R., A. Soda, Y. Saida, K. Sugihara, K. Takashima, et al., *Evaluation of the efficacy and safety of coil occlusion for patent ductus arteriosus in dogs.* Journal of Veterinary Medical Science, 2007. **69**(8): p. 857-859.

28. Henrich, E., N. Hildebrandt, C. Schneider, E. Hassdenteufel, and M. Schneider, *Transvenous coil embolization of patent ductus arteriosus in small (<= 3.0 kg) dogs.* Journal of Veterinary Internal Medicine, 2011. **25**(1): p. 65-70.

29. Blossom, J.E., J.M. Bright, and L.G. Griffiths, *Transvenous occlusion of patent ductus arteriosus in 56 consecutive dogs.* Journal of Veterinary Cardiology, 2010. **12**(2): p. 75 - 84.

30. Lloyd, T.R., R. Fedderly, A.M. Mendelsohn, S.K. Sandhu, and R.H. Beekman, *Transcatheter occlusion of patent ductus arteriosus with Gianturco coils.* Circulation, 1993. **88**(4): p. 1412-1420.

31. Miller, M., K. Meurs, S. Gordon, and E. Spangler. *Transarterial ductal occlusion using Gianturco vascular occlusion coils: 43 cases 1994-1998 (abstract).* In *Proceedings of the 17th Annual Veterinary Medical Forum*, ACVIM. 1999. Chicago, IL. p. 247.

32. Sreeram, N., M. Tofeig, K.P. Walsh, and P. Hutter, *Lung perfusion studies after detachable coil occlusion of persistent arterial duct.* Heart, 1999. **81**(6): p. 642-645.

33. Nguyenba, T.P. and A.H. Tobias, *The Amplatz canine duct occluder: A novel device for patent ductus arteriosus occlusion.* Journal of Veterinary Cardiology, 2007. **9**(2): p. 109-117.

34. Wilson, T.S., J.P. Bearinger, J.L. Herberg, J.E. Marion, W.J. Wright, et al., *Shape memory polymers based on uniform aliphatic urethane networks.* Journal of Applied Polymer Science, 2007. **106**(1): p. 540-551.

35. Lendlein, A. and S. Kelch, *Shape-memory polymers.* Angewandte Chemie-International Edition, 2002. **41**(12): p. 2034-2057.

36. Singhal, P., J.N. Rodriguez, W. Small, S. Eagleston, J.V. de Water, et al., *Ultra low density and highly crosslinked biocompatible shape memory polyurethane foams.* Journal of Polymer Science Part B-Polymer Physics, 2012. **50**(10): p. 724-737.

37. Rodriguez, J.N., Y.J. Yu, M.W. Miller, T.S. Wilson, J. Hartman, et al., *Opacification of shape memory polymer foam designed for treatment of intracranial aneurysms.* Annals of Biomedical Engineering, 2012. **40**(4): p. 883-897.

38. Rodriguez, J.N., F.J. Clubb, T.S. Wilson, M.W. Miller, T.W. Fossum, et al., *In vivo response to an implanted shape memory polyurethane foam in a porcine aneurysm model.* Journal of Biomedical Materials Research Part A, 2014. **102**(5): p. 1231-1242.

39. Small, I.V.W., P. Singhal, T.S. Wilson, and D.J. Maitland, *Biomedical applications of thermally activated shape memory polymers.* Journal of Materials Chemistry, 2010. **20**(17): p. 3356-3366.

40. Maitland, D.J., W. Small, J.M. Ortega, P.R. Buckley, J. Rodriguez, et al., *Prototype laser-activated shape memory polymer foam device for embolic treatment of aneurysms.* Journal of Biomedical Optics, 2007. **12**(3): p. 030504.

41. Heymann, M.A. and A.M. Rudolph, *Control of ductus arteriosus.* Physiological Reviews, 1975. **55**(1): p. 62-78.

42. Coceani, F. and P.M. Olley, *The response of the ductus arteriosus to prostaglandins.* Canadian Journal of Physiology and Pharmacology, 1973. **51**(3): p. 220-225.

43. Hamrick, S.E.G. and G. Hansmann, *Patent ductus arteriosus of the preterm infant.* Pediatrics, 2010. **125**(5): p. 1020-1030.

44. Michelakis, E., I. Rebeyka, J. Bateson, P. Olley, L. Puttagunta, et al., *Voltage-gated potassium channels in human ductus arteriosus.* Lancet, 2000. **356**(9224): p. 134-137.

45. Leonhardt, A., A. Glaser, M. Wegmann, D. Schranz, H. Seyberth, et al., *Expression of prostanoid receptors in human ductus arteriosus.* British Journal of Pharmacology, 2003. **138**(4): p. 655-659.

46. Schneider, D.J. and J.W. Moore, *Patent ductus arteriosus.* Circulation, 2006. **114**(17): p. 1873-1882.

47. Birchard, S.J., J.D. Bonagura, and R.B. Fingland, *Results of ligation of patent ductus-arteriosus in dogs - 201 cases (1969-1988).* Journal of the American Veterinary Medical Association, 1990. **196**(12): p. 2011-2013.

48. Jackson, W.F. and R.A. Henderson, *Ligature placement in closure of patent ductus arteriosus.* Journal of the American Animal Hospital Association, 1979. **15**(1): p. 55-58.

49. Rodriguez, J.N., M.W. Miller, A. Boyle, J. Horn, C.K. Yang, et al., *Reticulation of low density shape memory polymer foam with an in vivo demonstration of vascular occlusion.* Journal of the Mechanical Behavior of Biomedical Materials, 2014. **40**: p. 102-114.

50. Swensson, R.E., L.M. Valdescruz, D.J. Sahn, F.S. Sherman, K.J. Chung, et al., *Real-time doppler color flow mapping for detection of patent ductus arteriosus.* Journal of the American College of Cardiology, 1986. **8**(5): p. 1105-1112.

51. Singhal, P., A. Boyle, M.L. Brooks, S. Infanger, S. Letts, et al., *Controlling the actuation rate of low-density shape-memory polymer foams in water.* Macromolecular Chemistry and Physics, 2013. **214**(11): p. 1204-1214.

52. Hasan, S.M., J.E. Raymond, T.S. Wilson, B.K. Keller, and D.J. Maitland, *Effects of isophorone diisocyanate on the thermal and mechanical properties of shape-memory polyurethane foams.* Macromolecular Chemistry and Physics, 2014. **215**(24): p. 2420-2429.

53. Cohen, J., S.B. Litwin, A. Aaron, and S. Fine, *The rupture force and tensile strength of canine aortic tissue.* Journal of Surgical Research, 1972. **13**(6): p. 321-333.

54. Moriwaki, T., T. Oie, K. Takamizawa, Y. Murayama, T. Fukuda, et al., *Variations in local elastic modulus along the length of the aorta as observed by use of a scanning haptic microscope (SHM).* Journal of Artificial Organs, 2011. **14**(4): p. 276-283.

55. Eldredge, D.M., L.D. Carlson, D.G. Carlson, and J.M. Griffin, *Normal physiological data*, in *Dog owner's home veterinary handbook*, B. Adelman, Editor. 2007, Wiley Publishing, Inc: Hoboken, NJ. p. 573-574.

56. Wierzbicki, M.A., J. Bryant, M.W. Miller, B. Keller, and D.J. Maitland, *Mechanical and in vitro evaluation of an experimental canine patent ductus arteriosus occlusion device.* Journal of the Mechanical Behavior of Biomedical Materials, 2016. **59**: p. 156 - 167.

57. Horn, J., W. Hwang, S.L. Jessen, B.K. Keller, M.W. Miller, et al., *Comparison of shape memory polymer foam versus bare metal coil treatments in an in vivo porcine sidewall aneurysm model.* 2016.

58. Boyle, A.J., T.L. Landsman, M.A. Wierzbicki, L.D. Nash, W. Hwang, et al., *In vitro and in vivo evaluation of a shape memory polymer foam-over-wire embolization device delivered in saccular aneurysm models.* Journal of Biomedical Materials Research Part B-Applied Biomaterials, 2016. **104**(7): p. 1407-1415.

59. Landsman, T.L., R.L. Bush, A. Glowczwski, J. Horn, S.L. Jessen, et al., *Design and verification of a shape memory polymer peripheral occlusion device.* Journal of the Mechanical Behavior of Biomedical Materials, 2016. **63**: p. 195-206.

60. Tse, J.R. and A.J. Engler, *Preparation of hydrogel substrates with tunable mechanical properties.* Current Protocols in Cell Biology, 2010(SUPPL. 47): p. 10.16.11-10.16.16.

61. Robinson, R.A., L.H. Herbertson, S.S. Das, R.A. Malinauskas, W.F. Pritchard, et al., *Limitations of using synthetic blood clots for measuring in vitro clot capture efficiency of inferior vena cava filters.* Medical Devices: Evidence & Research, 2013. **6**: p. 49-57.

62. Jaeger, H.J., T. Mair, M. Geller, R.K. Kinne, A. Christmann, et al., *A physiologic in vitro model of the inferior vena cava with a computer-controlled flow system for testing of inferior vena cava filters.* Investigative Radiology, 1997. **32**(9): p. 511-522.

63. Jaeger, H.J., S. Kolb, T. Mair, M. Geller, A. Christmann, et al., *In vitro model for the evaluation of inferior vena cava filters: Effect of experimental parameters on thrombus-capturing efficacy of the Vena Tech-LGM filter.* Journal of Vascular and Interventional Radiology, 1998. **9**(2): p. 295-304.

64. Weems, A.C., J.E. Raymond, K.T. Wacker, T.P. Gustafson, B. Keller, et al., *Examination of radio-opacity enhancing additives in shape memory polyurethane foams.* Journal of Applied Polymer Science, 2015. **132**(23): p. 42054.

65. Weems, A., A. Boyle, and D.J. Maitland, *Two-year performance study of porous, thermoset, shape memory polyurethanes intended for vascular medical devices.* Smart Materials and Structures, 2017. **26**(3): p. 35054.

66. Agrawal, M., V.A. Sonetha, S. Sharma, S. Parakh, B. Dalvi, et al., *Evolution of a novel intraductal patent ductus arteriosus occlusion device.* Journal of Medical Devices-Transactions of the ASME, 2011. **5**(3): p. 035001.

67. Echigo, S., T. Matsuda, T. Kamiya, E. Tsuda, K. Suda, et al., *Development of a new transvenous patent ductus arteriosus occlusion technique using a shape memory polymer.* ASAIO Transactions, 1990. **36**(3): p. M195-198.

68. Stauthammer, C.D., J. Olson, D. Leeder, K. Hohnadel, M. Hanson, et al., *Patent ductus arteriosus occlsuion in small dogs utilizing a low profile Amplatz canine ductal occluder prototype.* Journal of Veterinary Cardiology, 2015. **17**(3): p. 203-209.

69. Duerig, T.W., D.E. Tolomeo, and M. Wholey, *An overview of superelastic stent design.* Minimally Invasive Therapy & Allied Technologies, 2000. **9**(3-4): p. 235-246.

70. MacWilliams, J., *Optimization of nitinol shape setting through post laser cutting processing*, in *Medical device materials III: Proceedings from the Materials & Processes for Medical Devices Conference 2005*, R. Venugopalan and M. Wu, Editors. 2006, ASM International: Materials Park, OH. p. 69-72.

71. Paprottka, K.J., P.M. Paprottka, M.F. Reiser, and T. Waggershauser, *Comparative study of the corrosion behavior of peripheral stents in an accelerated corrosion model: experimental in vitro study of 28 metallic vascular endoprostheses.* Diagnostic and Interventional Radiology, 2015. **21**(5): p. 403-409.

72. Stoeckel, D., A. Pelton, and T. Duerig, *Self-expanding nitinol stents: material and design considerations.* European Radiology, 2004. **14**(2): p. 292-301.

73. Schuessler, A. and M. Strohel, *Status and trends of nitinol micromachining techniques*, in *SMST-2003: Proceedings of the International Conference on Shape Memory and Superelastic Technologies*, A.R. Pelton and T. Duerig, Editors. 2004, SMST Society Inc: Menlo Park, CA. p. 135-141.